Hydrogeology Journal
https://doi.org/10.1007/s10040-025-02952-w

PAPER

Characterization of an onshore–offshore aquifer system in the Venetian Friulian Plain and north Adriatic Basin: a 3D modeling approach

Cristina Corradin[1,3] · Ariel T. Thomas[2] · Angelo Camerlenghi[3] · Luca Zini[1] · Michela Giustiniani[3] · Martina Busetti[3] · Laura Foglia[4] · Claudia Bertoni[5] · Aaron Micallef[2,6]

Received: 23 July 2024 / Accepted: 25 August 2025

Abstract

Continental coastal aquifer systems are well-studied worldwide and are often characterized on the basis of extensive and diverse borehole datasets. However, while it is postulated that in some cases, these aquifers may extend offshore, their seaward reach remains widely unknown due to the frequently limited availability of data, particularly for subsurface sediments and their pore water salinity. This paper presents a valuable characterization of the onshore aquifers in the Venetian-Friulian Plain (northeastern Italy) and their offshore extension in the Northern Adriatic Shelf, within ~20 km from the coastline. Three-dimensional digital geological and stratigraphic modeling was used to investigate geometries of the layered artesian aquifer system hosted in the Middle to Late Pleistocene sedimentary succession. Near-coastal and offshore aquifers are found to have mainly formed during coastline migration driven by sea level changes and low-permeability layers, sealing these aquifers, result from fine alluvial sediments during sea level lowstands or fine marine sediments during highstands. This study suggests that Quaternary glacio-eustatic fluctuations are mainly responsible for the genesis of the layered aquifer system in the study area. Given the consistency of depositional processes active in the Northern Adriatic Basin since Middle-Pleistocene, and that coastal fresh groundwater extends hundreds of meters below the topographic surface, this study confirms that the Northern Adriatic Basin has significant potential to host widespread offshore freshened groundwater aquifers. This resource might represent an additional freshwater supply in the future.

Keywords Coastal aquifers · Geological modeling · Geostatistics · Venetian Friulian Plain · North-eastern Adriatic Sea

Introduction

Groundwater utilization dates from ancient times and presently sustains 50% of the global urban population as an essential resource for human consumption, agriculture, and industry (United Nations 2022). It is primarily investigated in terrestrial contexts; however, recent studies (e.g. Post et al. 2013; Micallef et al. 2021) shed light on the potential of continental shelves to host large amounts of offshore freshened groundwater (OFG). The interest in OFG is primarily associated with the prospect of utilization which could present an important additional water resource in the future, either for direct use or for desalination purposes. Since OFG is a new hydrogeological frontier there is still a poor understanding of its distribution, timing, and the controlling factors for its occurrence (Micallef et al. 2021). Although OFG aquifers may exhibit several genetic and emplacement mechanisms,

Published in the special issue "Advances in understanding offshore freshened groundwater".

✉ Cristina Corradin
cristina.corradin@phd.units.it

1 Department of Mathematics and Geosciences, University of Trieste, Trieste, Italy

2 Department of Geosciences, Faculty of Science, University of Malta, Msida, Malta

3 National Institute of Oceanography and Applied Geophysics, Trieste, Sgonico, Italy

4 Department of Land Air and Water Resources, University of California, Davis, CA, USA

5 Department of Earth Sciences, University of Oxford, Oxford, UK

6 Monterey Bay Aquarium Research Institute, Moss Landing, CA, USA

the most common is meteoric recharge during the sea level lowstands (Micallef et al. 2021).

This study investigates the geological and stratigraphic framework of the Pliocene and Quaternary sediments of the Venetian Friulian Plain (VFP), an Italian region hosting a layered, confined aquifer system that lies hundreds of meters below the ground level. In light of the interest in alternative freshwater sources such as OFG, the scope of this study was extended to the nearshore sector of the Northern Adriatic Basin (NAB), offshore from the VFP.

Onshore groundwater is often a vulnerable resource suffering significant pressure due to growing consumption, climate change, waste from pipeline leakage and other sources of contamination. In the VFP, groundwater resources are threatened by numerous factors. The most important is anthropogenic, in particular the over-exploitation of artesian flowing wells and the unsustainable utilization of surface waters (Zini et al. 2023). The exploitation rate from these aquifers is estimated at 48.6 m^3/s, while the recharge rate is about 43.7 m^3/s, which threatens the future freshwater availability (Zini et al. 2023) and promotes saline water intrusion (Goswami et al. 2020). In addition to excessive exploitation, the escalation in both the intensity and frequency of extreme rainfall events in recent years due to climate change (ARPA FVG 2018) has led to a reduction of groundwater recharge and an increase in surface runoff (Horton et al. 1940; Dunne et al. 1983; Bronstert et al. 2023).

From 1961 to 2016, the average temperature rose by 0.3 °C per decade (ARPA FVG 2018), leading to a growing evapotranspiration deficit and an increased water demand, especially in the summer season.

One of the biggest challenges to avoid long-term aquifer depletion is to gain a comprehensive knowledge of the aquifer recharge mechanisms and thus adapt utilization to a sustainable rate. To achieve this, the comprehensive knowledge of aquifer characteristics is a fundamental tool for quantifying, managing, and monitoring groundwater availability (Canter 1982). This includes knowledge of sedimentary architectures and lithological characteristics, which can be obtained through advanced aquifer characterization techniques. These techniques include data acquisition methods such as geophysical surveying and borehole logging, as well as interpretative approaches like geological and petrophysical modeling (Maliva 2016). Previous studies in the area have primarily examined onshore aquifers (Zini et al. 2023), while the offshore sector remains poorly investigated. Amadori et al. (2020) presented a broad stratigraphic overview encompassing both coastal onshore and offshore areas in the western sector of the northern Adriatic Basin, albeit not specifically focused on aquifers. Therefore, a comprehensive three-dimensional geological and stratigraphic overview of the onshore–offshore region of the VFP and its NAB counterpart remains missing.

This paper aims to investigate geometries, architectures, and the origin of the complex aquifer system hosted in the Middle to Late Pleistocene siliciclastic sedimentary sequences of the VFP, including the coastal zone and the offshore area of the NAB as a "continuum" of the onshore subsurface water network. The subsurface is characterized by developing four three-dimensional models thereby presenting a comparison of different modeling approaches. These include (1) a deterministic lithostratigraphic data interpolation model using Leapfrog GEO (provided by Seequent); (2) a stochastic geostatistical model using Petrel 2021 (from Schlumberger); (3) a trend model of aquifers geometries independent of lithological data; and (4) a 3D model of sedimentary sequences associated with Pliocene to Quaternary sea level fluctuations based on literature and reinterpreted borehole stratigraphic description.

This article is the first part of a wider research project on characterizing OFG across the NE Adriatic shelf, which follows an established two-step workflow, used for studying OFG on several worldwide continental margins (Micallef et al. (2020) for the New Zealand offshore; Lipparini et al. (2023) for offshore Sicily, Italy; Sheng et al. (2023) for the Pearl River Estuary in South China). This workflow includes, first, the modeling and characterization of the aquifers from a geological perspective (including lithology, stratigraphy, and physical properties of sediments, including permeability) and, second, the modeling of hydrogeological aspects relevant to groundwater flow simulations (Corradin 2025).

Geological setting

The study area is located in north-eastern Italy, between the southern Alps piedmont and the northern Adriatic Sea. It comprises the eastern portion of the VFP and the NAB (Fig. 1). The area is approximately 80 km long and 60 km wide (Fig. 1a). It is bounded to the NW and NE by the active NE to SW-oriented alpine fold and thrust systems, and by the active NW to SE-oriented fold and thrust system underlying the Friulian Plain, respectively (Marchesini et al. 2023). To the south, the study area is bounded by the northern tip of the Adriatic Italian Economic Exclusive Zone (EEZ) and to the west by the western portion of the VFP (Fig. 2a).

Together with the NAB, the VFP lies on the Adria Microplate, an African tectonic plate associated with the continental collision with Eurasia (Dercourt et al. 1986; Robertson and Grasso 1995). This area is the foreland of three different orogens (the Apennines, the Alps, and the Dinarides), which developed along three independent subduction zones. The orogenic activity surrounding the north Adriatic Plate persists, although Apennines subduction dominates, dictating the asymmetric subsidence in the northern Adriatic

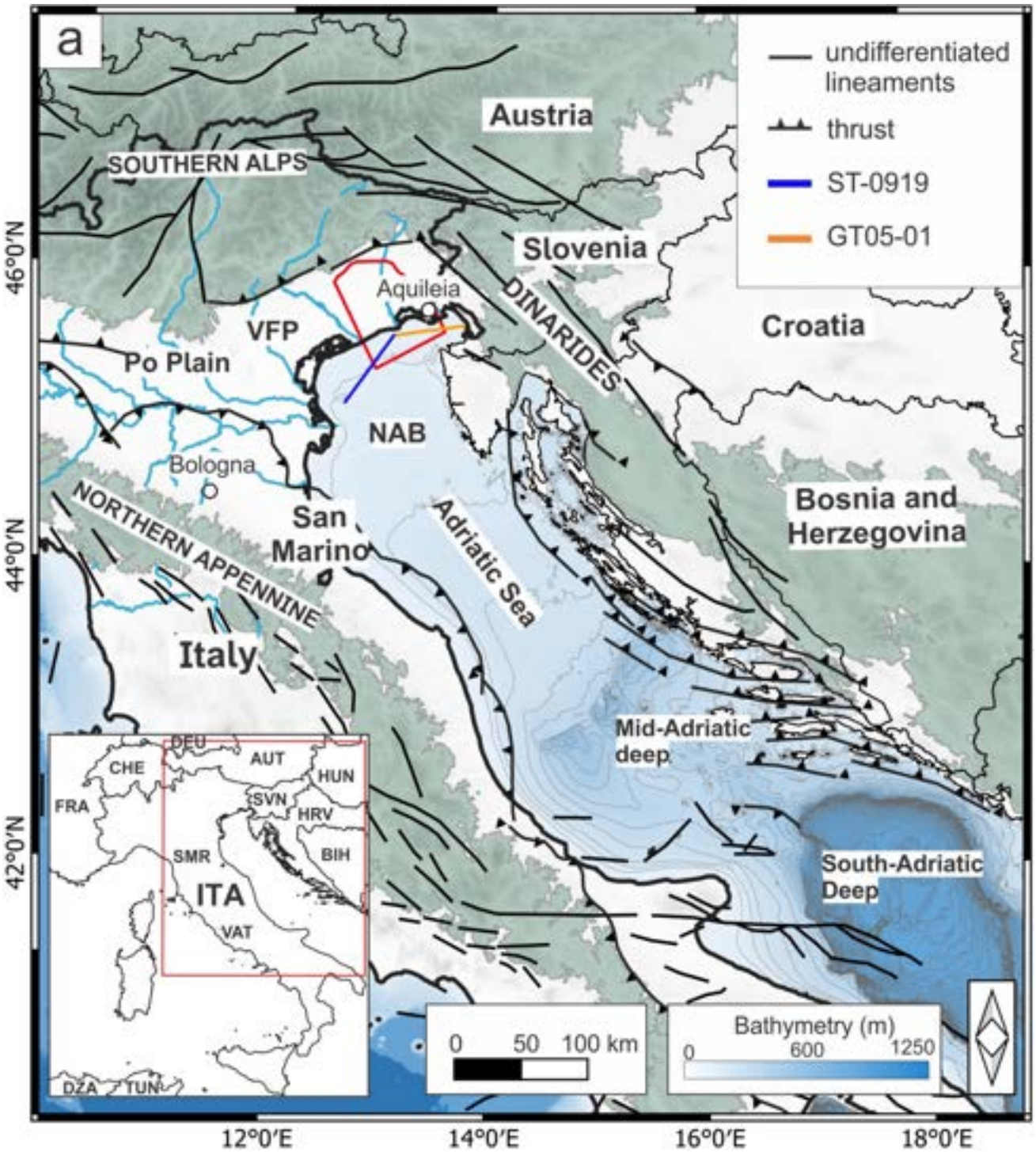

Fig. 1 (**a**) Simplified structural geology map of the Adriatic Basin and surrounding landmasses. The study area (*solid red line*) is surrounded by External Dinarides to the east and Southern Alps to the north. Tectonic lineaments, including major undifferentiated faults and thrusts in Italy and surrounding regions are modified after Palano (2015). Seismic lines ST09-19 and GT05-01 are sourced from Zecchin et al. (2022). (**b**) Plio-Quaternary stratigraphic sequences of seismic lines ST09-19 and GT05-01 and main stratal surfaces, including the Late Gelasian Surface (LGS), which marks a major drowning event dated at 1.86 Ma (modified after Zecchin et al. 2022). The vertical axis is expressed in two-way travel time (TWT)

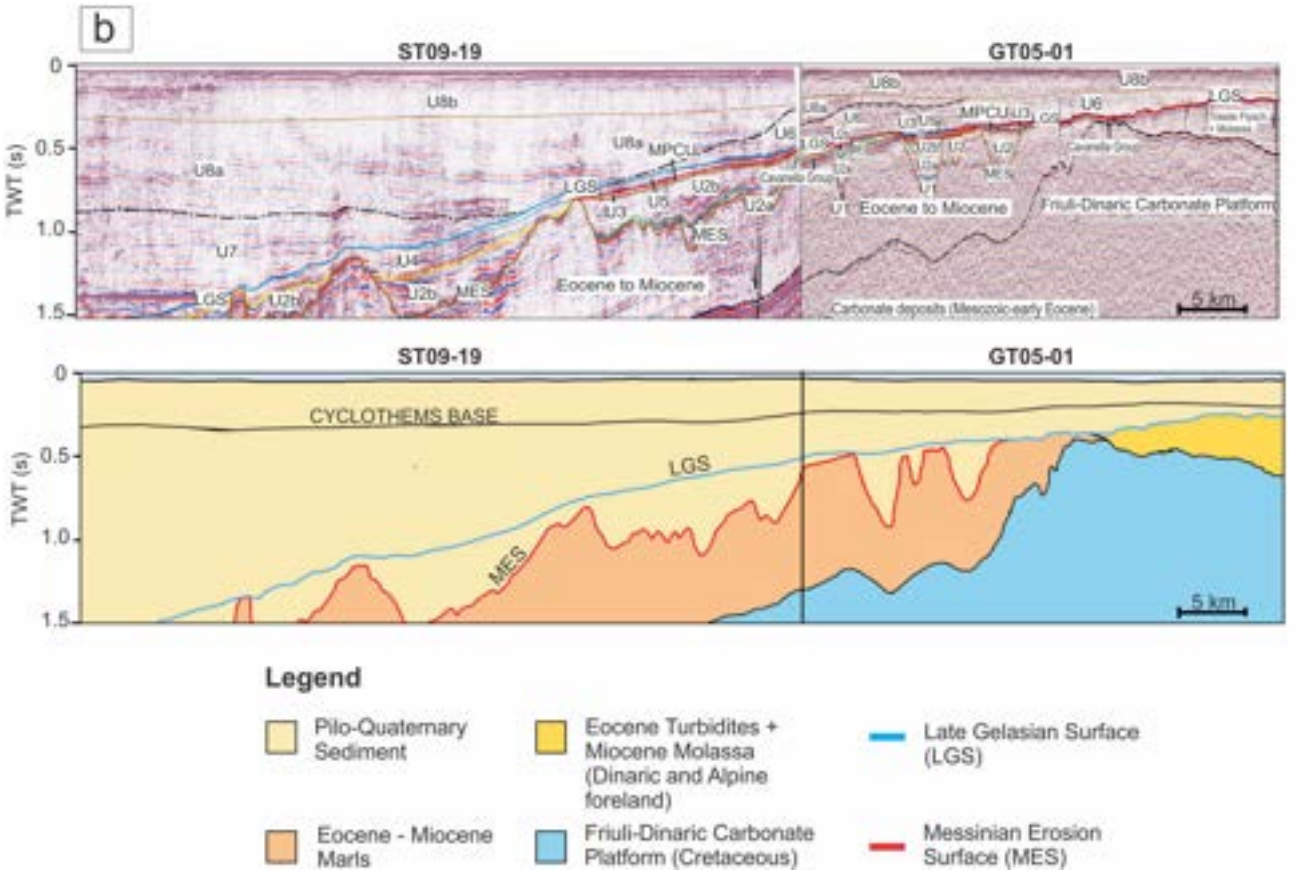

Fig. 1 (continued)

region (Cuffaro et al. 2010; Livani et al. 2023) and producing a wedge-shaped Pliocene to Quaternary sedimentary unit (Zecchin et al. 2022). The maximum thickness of these sediments is ca. 2 km in the south-western portion of the Venice Lagoon and decreases toward the east (Carminati et al. 2003; Zecchin et al. 2022) (Fig. 1b).

It is important to note that the study area borders the eastern edge of the Po Plain and the western sector of the NAB, where the subsurface structure is well-constrained thanks to extensive geophysical and geological data sets primarily originating from hydrocarbon exploration (e.g., Amadori et al. 2019, Livani et al. 2023), and the offshore sedimentary evolution has been extensively studied through high-resolution seismic reflection surveys and coring (e.g., Amorosi et al. 2016; Ronchi et al. 2018; Campo et al. 2024). The VFP and the eastern sector of the NAB, which are comparatively lacking in subsurface data, feature a different structural setting and sedimentary evolution with respect to the Po Plain. This is mainly due to a much lower subsidence rate (e.g., Carminati et al. 2003) due to the influence of the Dinaric system in the geodynamic evolution of the VFP (e.g., Zecchin et al. 2022; Brancatelli et al. 2023), as well as a contrasting surface hydrography (e.g., Fontana et al. 2008). These factors result in a significantly lower riverine sedimentary input to the marine basin (e.g., Correggiari et al. 1996).

The Venetian Friulian Plain (VFP)

The main sediment sources feeding the VFP are the Southern Alps and the External Dinarides. The eastern portion of the VFP is characterized by a network of rivers that originate in the Alpine and Pre-Alpine regions and flow southward toward the Adriatic Sea (Fig. 2a). The sedimentary dynamics of these rivers play a crucial role in shaping the landscape of the plain. Conical-shaped alluvial fans and megafans extend into the plain from the outlets of the major valleys of the southern Alps Piedmont (Mancin et al. 2007; Fontana et al. 2008, 2010). Their Late Pleistocene and Holocene evolution were mainly controlled by climatic changes and eustasy with a southward aggrading phase related to glacial periods (Fontana et al. 2010). The last alluvial depositional phase dates to the Last Glacial Maximum (LGM) and was followed, after 20,000 years BP, by a marked reduction in rates of deposition accompanied by strong alluvial incision.

The VFP can be divided into two hydrogeologically different areas: the High Plain (HP) and the Low Plain (LP) (Fig. 2a,b) separated by the resurgence belt (see below). A conceptual representation of the HP and LP hydrogeological settings is given in Fig. 2b. The HP extends 10–25 km from the mountain front and has a relatively steep topographic gradient (0.3–0.7%). It is mainly composed of gravel, associated with megafans development, and hosts a thick phreatic aquifer. The LP extends from the resurgence belt to the coastline and has a lower topographic gradient (0.1%). Here, alternating layers of high permeability (mainly sand) and low permeability (silt/clay) reflect varying depositional environments, from fluvial/alluvial to lagoon and coastal settings resulting in the formation of 11 to 12 confined aquifers that reach a depth of 500 m below sea level (Zini et al. 2011; Cucchi et al. 2008; Marcolla et al. 2021). Confined aquifers have an average thickness of 15 m and are separated by 10 to 40 m thick confining units (aquitards) (Zini et al. 2023). The five shallowest aquifers are located approximately within the first 250 m below ground level. The resurgence belt (e.g., Cucchi et al. 2008; Fig. 2a,b) marks the transition between the High and Low Plains. It is an approximately east–west elongated area characterized by the widespread occurrence of springs of groundwater from the HP that encounters a less permeable medium in the sediments of the LP (Martelli and Granati 2006; Zini et al. 2011). Mountain recharge and infiltration of precipitation in the HP are the primary water sources for the confined aquifers downstream. Overflow from the HP feeds the belt of resurgences, a distinctive drainage system called the resurgence river system. Resurgence and alpine rivers generate a surface water flow in the LP and into the northern Adriatic Sea.

A peculiarity of the northern Adriatic coastline in Italy is the presence of lagoons, particularly unstable and fragile transitional areas, comprising a variety of different habitats of unique environmental and eco-systemic value (Fontolan et al. 2012). The northern Adriatic Sea hosts two major lagoons, the Venice Lagoon and the Grado-Marano Lagoon.

The location of the maximum flooding surface and paleo lagoon deposits from the Middle Pleistocene (MIS-7 interglacial) to the present has been reconstructed in the subsurface of the VFP from borehole studies (Marcolla et al. 2021; Fontana et al. 2010; Carton et al. 2009; Zecchin et al. 2017). Evidence of the transgression is found progressively landward with time, reaching 25 km from the present coastline about 20 km landward of the coastline below the present course of the Tagliamento River, in the case of MIS-7 interglacial (Fig. 2a).

The Northern Adriatic Basin (NAB)

The Adriatic Sea overlies the largest low-gradient epicontinental shelf in the Mediterranean area with a lateral extension of ca. 800 × 200 km (Fig. 1a). The seafloor of the northern sub-basin (the NAB), reaches 100 m below sea level, with an extremely gentle bathymetric gradient along the major axis (ca. 0.035%) (Russo and Artegiani 1996; Cattaneo et al. 2007). Presently, it is subject to micro-tidal and storm-dominated regimes, characterized by a cyclonic thermohaline circulation that forces riverine waters to flow counter-clockwise along the basin's western side, in a southerly direction (Malanotte-Rizzoli and Robinson 2012). Together with tidal erosion and wave-induced currents, these factors determine the morphology of the coastal areas.

The terrigenous sediment source in the NAB is almost exclusively fluvial, with very little or absent aeolian supply (Colantoni et al. 1979). In the study area, the rivers draining the eastern Alps (Adige, Brenta, Piave, Tagliamento, Isonzo) carry mainly detrital carbonates (Vdovic and Juracic 1993; Covelli et al. 2004) and contribute 3.0×106 tons per year altogether to the NAB. The present fluvial supply originating from the Dinarides is essentially negligible. By comparison, the Po River alone, discharging in the western sector of the NAB transports material eroded from the Central and Western Alps and the northern Apennines, contributes a sediment flux to the basin of 3.9×10^7 tons per year (Correggiari et al. 1996).

Figure S1a of the electronic supplementary material (ESM) shows the present-day grain size distribution of seafloor sediments in the eastern sector of the NAB, highlighting nearshore areas characterized by silt and clay deposits, representing the primary rivers' asymmetric prodeltas (e.g., the Tagliamento and Isonzo rivers' pro-deltas). Conversely, farther away from the coast, large coarse sandy deposits (95% sand content) are relict paleo-shorelines formed during the Holocene transgression (Brambati et al. 1983; Colantoni et al. 1979; Zecchin et al. 2015). These deposits are still exposed at the seafloor because of the persistent alongshore drift currents that cause along-shore dispersion of fine-grained sediments into the Meso-Adriatic Deep (Brambati et al. 1983). Laterally continuous and amalgamated coastal sands located in the proximal sector of the basin are generally linked to highstand periods or onset of falling sea-level (Fontana et al. 2010, their Fig. 2). Two generations of incised valleys exist offshore the Venice Lagoon, east of the study area, originated by fluvial erosion and subsequent infill during the Last Glacial Maximum exposure of the NAB, and by tidal inlets and channels during the establishment of a transgressive lagoon environment in the early Holocene (Ronchi et al. 2018).

The first study concerning the occurrence of nearshore NAB aquifers was proposed by Giustiniani et al. (2022) which highlighted the potential middle-late Pleistocene sediments of the NAB to host fresh, or freshened aquifers through the analysis of seismic reflection lines and the seismo-stratigraphic sequences analysis. Evidence of several

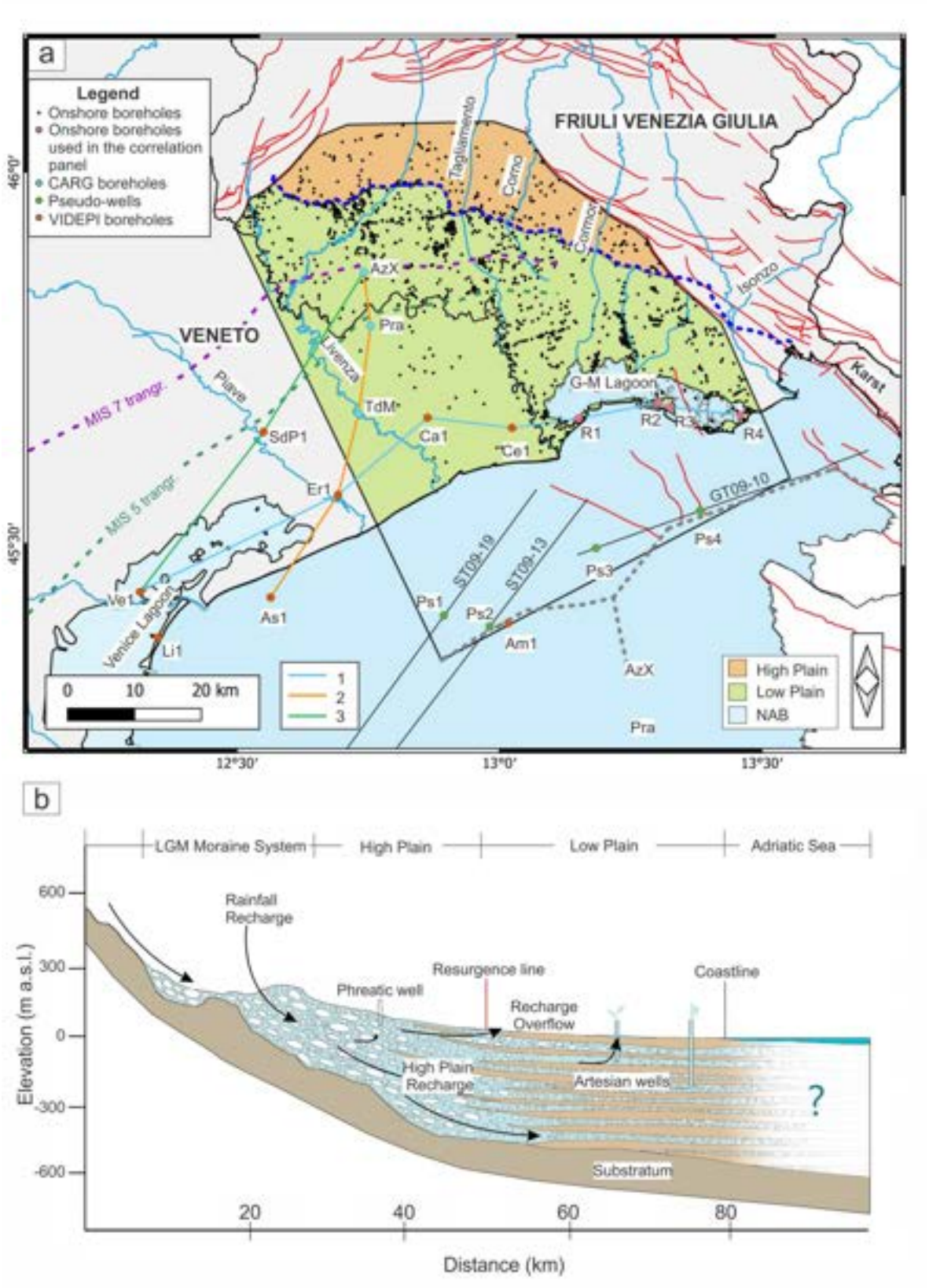
a
Legend
Onshore boreholes
Onshore boreholes used in the correlation panel
CARG boreholes
Pseudo-wells
VIDEPI boreholes
FRIULI VENEZIA GIULIA
VENETO
Tagliamento
Como
Cormor
Isonzo
Karst
Livenza
Piave
MIS 7 trangr.
MIS 5 trangr.
G-M Lagoon
Venice Lagoon
AzX
Pra
TdM
Ca1
Ce1
SdP1
Er1
Ve1
As1
Li1
R1
R2
R3
R4
GT09-10
ST09-19
ST09-13
Ps1
Ps2
Ps3
Ps4
Am1
0 10 20 km
1
2
3
High Plain
Low Plain
NAB
46°0'
45°30'
12°30'
13°0'
13°30'
b
LGM Moraine System
High Plain
Low Plain
Adriatic Sea
Rainfall Recharge
Phreatic well
Resurgence line
Recharge Overflow
Coastline
High Plain Recharge
Artesian wells
Substratum
Elevation (m a.s.l.)
600
300
0
-300
-600
20
40
60
80
Distance (km)

◂**Fig. 2** (**a**) Overview of the study area and the location of the main dataset. The figure depicts: Faults (*red lines*) (Marchesini et al. 2023), the resurgence line (*dashed blue line*), the main hydrography (*solid blue lines*), the EEZ (*solid gray line*), seismic profiles (*solid black lines*), the MIS 7 and MIS 5 marine transgressions (*dashed purple and green lines*), modified after Marcolla et al. (2021). The traces of cross-correlation panels: 1 Along-Coast correlation panel; 2 Onshore–Offshore Correlation Panel; and 3 Venezia1–Azzano Decimo Correlation Panel. Borehole names have been abbreviated as follows: Ve1. Venezia 1; SdP1, San Donà di Piave 1; Er 1, Eraclea 1; Ca1, Cavanella 1; Ce1, Cesarolo 1; AzX, Azzano Decimo; TdM, Torre di Mosto; Pra, Pramaggiore. R1, R2, R3, R4 is a subgroups of the regional dataset. (**b**) Conceptual model of a transect of the study area (modified after Zini et al. 2011)

hundreds of meters of freshwater-saturated sediment is provided by hydrocarbon well VIDEPI Assunta 1 (see the *Input dataset* section).

Cyclothems

Since the Middle Pleistocene Transition (MPT), both the NAB and the southern portion of the VFP have experienced several cyclical sea level fluctuations and consistent depositional processes (Massari et al. 2004; Amadori et al. 2020). Regressive–transgressive (R-T) cycles led to the deposition of sequences of shallow-marine (i.e., shoreface, innershelf, prodelta) to continental (i.e., aeolian, fluvial, floodplain) facies named "cyclothems" (Amadori et al. 2020). R-T frequency is related to the periodicity of glaciations and astronomical cyclicity, which changed from being dominantly 40 ka before the MPT (obliquity-dominated) to 100 ka afterward (eccentricity-dominated) (Shackleton 1997). Within this framework, each cyclothem serves as a sedimentary archive encompassing the interval between consecutive odd (interglacial) marine isotopic stages (MIS—Martinson et al. 1987). The shallowest five cyclothems correspond to sedimentary representations of MIS 5 to 1, 7 to 5, 9 to 7, 11 to 9, and 13 to 11, respectively. Cyclothems record variations in sedimentary bodies geometries and grain size, reflecting changes in accommodation space and depositional environment. The lowest portion of a cyclothem records the falling stage systems tract (FSST) followed by a lowstand systems tract (LST), reflecting the stratigraphic transition from shallow marine to littoral and continental deposits. In its shallower and transgressive portion, each cyclothem records the shift from continental to littoral and shallow marine environments during the transgression and the following sea-level highstand phases (transgressive system tract—TST, highstand system tract—HST). Moreover, an overall regressive trend due to the progressive infilling of the NAB is represented by a trend of upward increase of continental sedimentary facies (Amadori et al. 2020). The southward and northward shifting of the shoreline during Quaternary R-T cycles likely occurred parallel to the present-day arcuate coastline. For the last R-T cycle, this is evidenced by the shape of the last glacial maximum shelf break, currently located at the mid-Adriatic deep and by the telescoped transgressive and regressive parasequences in the geological record (e.g., Correggiari et al. 1996; Storms et al. 2008; Amorosi et al. 2016). Similar, though less precisely mapped, previous coastline migrations are described by Marcolla et al. (2021), Fontana et al. (2010), Carton et al. (2009), and Zecchin et al. (2017). A reconstruction of the marine transgression limits from the last two cycles is shown in Fig. 2a.

Eccentricity-dominated cyclostratigraphy since MPT has been investigated by several authors in the NAB and VFP (Massari et al. 2004; Zanferrari et al. 2008; Bresolin 2013; Marcolla et al. 2021; Fontana et al. 2010; Fontana et al. 2012; Amorosi et al. 2016; Campo et al. 2017; Amadori et al. 2020; Zecchin et al. 2022) and in the Central Adriatic Basin (Trincardi and Correaggiari 2000; Ridente and Trincardi 2002; Piva et al. 2008). Onshore, the two deepest borehole stratigraphies interpreted for R-T cycles are Venezia 1 (950 m bsl) and Azzano Decimo borehole (271 m bsl), respectively. The Venezia 1 borehole is located on the coast and shows five major R-T cycles, each 30–75 m thick, formed by the cyclic alternation of coastal or deltaic, lagoonal, fluvial, floodplain deposits and overlying shallow marine or shelf facies. The third cycle from the top is represented by two minor obliquity-based cycles of 40k years (Massari et al. 2004; Amadori et al. 2020). The Azzano Decimo well is located approximately 34 km landward from the coast and was interpreted for eight R-T sequences in the upper 260 m (Fig. 2a). In the Azzano Decimo well, the last transgression-related sediments are not recorded because the last interglacial maximum flooding surface is located southward (Zanferrari et al. 2008). Offshore, cyclothems comprehensive sequence base have been seismically interpreted and corresponds to the U8b unit identified by Zecchin et al. (2022) (Fig. 1b).

Materials and methods

Input dataset

Within the study area, the bulk of the information comes from the regional hydrological borehole dataset compiled by the University of Trieste (Fig. 2a). The borehole dataset contains data from the hydrological well database of the Geological Survey and Hydrological Resource Management Survey of the Friuli Venezia Giulia Autonomous Region, the Italian Institute for Environmental Protection and Research (ISPRA) and the Friuli Venezia Giulia Regional Environmental Protection Agency (ARPA FVG). An additional set of hydrological well data was provided by the company Livenza Tagliamento Acque (LTA) S.p.A.

that manages potable water abstraction and distribution in the study area. Finally, publicly available well data from the Geologic Cartography of Italy Project (CARG) and the Visibility of Petroleum Exploration Data in Italy Project (ViDEPI) were used (Fig. S1b of the ESM). Regarding the boreholes, 1626 onshore boreholes feature lithostratigraphic data and 5164 boreholes provide information on wells screen depth (Fig. S1b,c of the ESM). The well screen is the windowed section of the well casing through which water can enter the pipe and indirectly provides the approximate thickness of a high permeability layer. When the depth of the screen was not available, it was assumed to be the maximum well depth in accordance with Zini et al. (2011). This approximation is justified by the fact that drilling above the target freshwater-bearing layer is ineffective, while drilling far beyond an aquifer is economically and technically unnecessary. The reliability of the stratigraphic dataset is significantly affected by variations in the year of acquisition, depth targets and drilling objectives. Most of these boreholes, which focus on shallow depths, were drilled primarily for freshwater supply purposes, while the deeper wells are typically for geothermal resource energy utilization or hydrocarbon exploration. For the Venezia 1 (Massari et al. 2004), Azzano Decimo (Zanferrari et al. 2008), Torre di Mosto and Pramaggiore boreholes, a detailed analysis of the depositional facies is available in addition to hydrological information (Fontana et al. 2010; Fontana et al. 2012). Four onshore wells (Venezia 1, Eraclea 1, Cesarolo 1, Cavanella 1) and one offshore well (Assunta 1), were drilled for hydrocarbon exploration, provide spontaneous potential, and resistivity logs. The published multichannel seismic reflection lines considered for this study are GT09-10 from OGS seismic profiles collected by the R/V OGS Explora in the Gulf of Trieste and ST 09–19 and ST09-13 from the STENAP dataset (Donda et al. 2013; Zecchin et al. 2022) (Fig. 2a).

Pseudo-stratigraphic logs and seismic-borehole ties with respect to cyclothems

The offshore portion of the study area has significantly less data coverage than the onshore counterpart. Four offshore pseudo-stratigraphic logs (PS1, PS2, PS3, PS4) were generated to better constrain the model. These pseudo logs provided a simplified representation of the area's stratigraphy, capturing lithological variations associated with cyclothems. The pseudo logs are located along seismic lines that were previously used for the identification of the cyclothem sequence by Zecchin et al. (2022) (refer to the "Cyclothems" section). The maximum depth of the pseudo log is therefore set equal to the base of the cyclothems. Within the cyclothem unit, four reflectors corresponding to the base of each cyclothem were interpreted for the two western pseudo-wells (PS1, PS2) located on seismic lines ST09–13B and ST09-19. These reflectors were later converted from time to depth using a velocity of 1700 m s^{-1} for Quaternary sediments (Dal Cin et al. 2022). Eastward, in the pseudo-stratigraphic logs PS3 and PS4, the thickness of the cyclothems falls below the resolution of the seismic data. As a result, each individual cyclothem was assumed to have a uniform thickness down to the unit's basal surface. Each cyclothem was assigned a stratigraphy representing a complete R-T cycle, with the relative thickness of lowstand, falling stage, transgressive highstand systems tract (LST + FSST, TST and HST) inferred from the Venezia 1 well cyclothem 5, as summarized in Fig. 3. This stratigraphic framework was then applied to all cycles in the pseudo logs.

The utilization of pseudo logs to improve the property prediction has been widely proven to be a useful approach for reservoir facies modeling (e.g., Ayeni et al. 2008; Connolly and Hughes 2016; Liu et al. 2020). However, their representativeness is inherently constrained by assumptions regarding lateral continuity and stratigraphic simplifications. The utilization of pseudo logs in this study includes two main assumptions: (1) the stratigraphy of the Venezia 1 well extends uniformly from the western to the eastern portions of the NAB, and (2) cyclothem 5 of the stratigraphic record of Venezia 1 is representative of all cyclothems in the pseudo stratigraphic logs. The first assumption is made according to the description of the cyclothem sequence by Zecchin et al. (2022) and Amadori et al. (2020), which represents a laterally continuous sedimentary succession of sub-parallel units for the entire northern Adriatic Basin. The second assumption is based on the different relative positions of the Venezia 1 well and the pseudo logs within the basin. Venezia 1 was chosen as the reference because it is the closest borehole with a detailed stratigraphic interpretation, capturing the transition from continental to marine environments over Plio-Quaternary sea-level fluctuations. However, as suggested by Amadori et al. (2020), progressive sediment input during the Plio-Quaternary caused the Venezia 1 site to become increasingly shallow, reducing the influence of sea-level fluctuations on its depositional history. Since the pseudo stratigraphic logs are located offshore, where deeper depositional settings prevailed, cyclothem 5, the deepest identified cyclothem in Venezia 1, was selected as the reference. This choice ensures that the reference cyclothem reflects conditions more comparable to the offshore locations of the pseudo logs. The utilization of pseudo logs might introduce uncertainties on basin infilling, sediment supply variations, and differential subsidence that may have led to localized deviations from the assumed depositional framework. Nevertheless, this level of simplification was considered to be appropriate in this case given the fact that the study area, in the eastern portion of the north Adriatic Basin, underwent a uniform sedimentary and tectonic history. The construction of these logs is based on previous

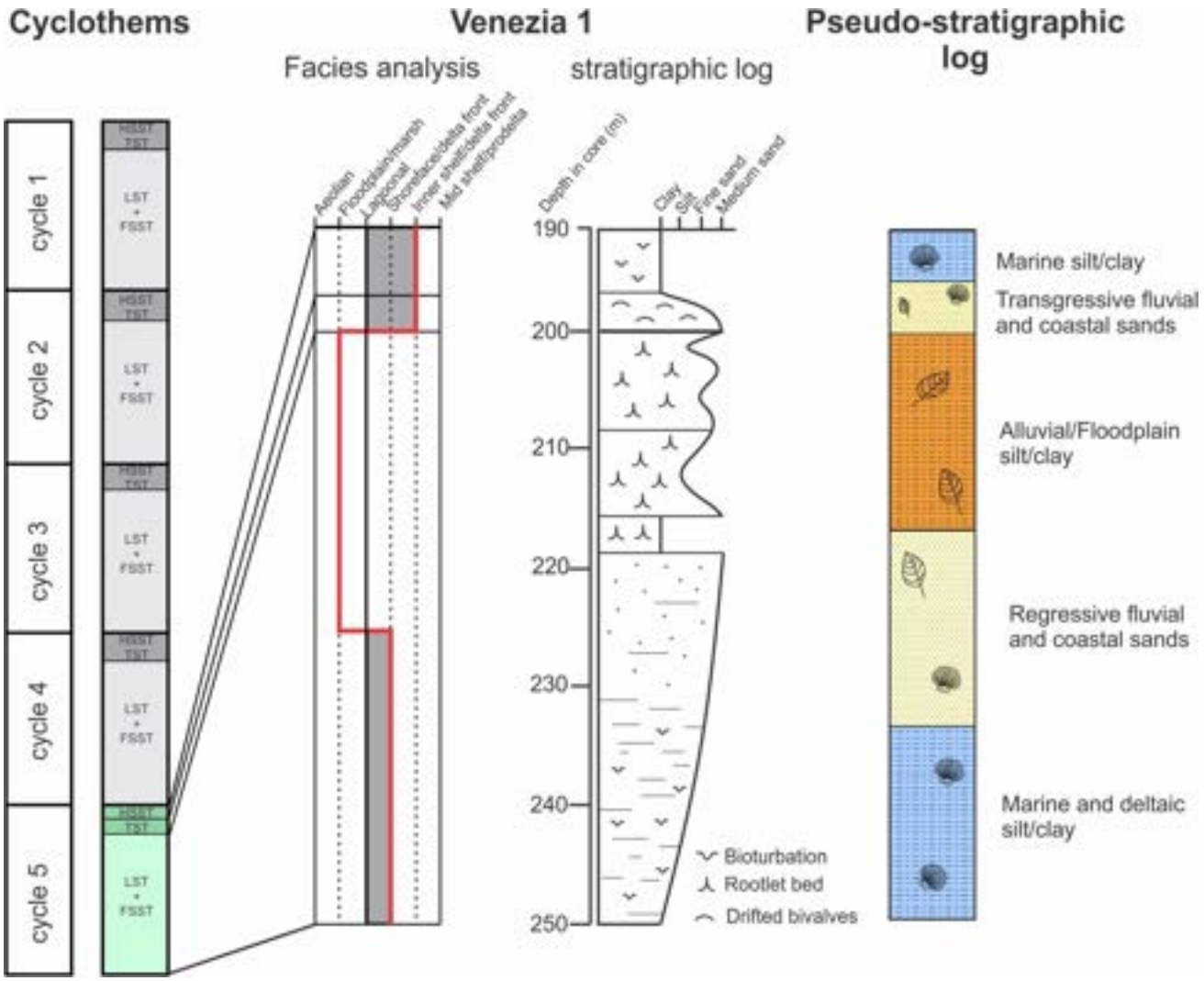

Fig. 3 Conceptual representation of a pseudo-stratigraphic log. (left) a conceptual borehole exhibits five successive R-T cycles with constant thickness, each composed of a regressive phase (FSST + LST) and a transgressive phase (TST + HST). Thickness proportions are derived from the 5th cycle recorded in Venezia 1 (Amadori et al. 2020), whereas the regressive phase constitutes 85% of the cycle thickness. (right) illustration depicting the magnified view of a sedimentary sequence for one cycle, along with the assumed sedimentary depositional environment. Given the limited literature, the coastal deposits of regressive phases are simplified and assumed to be as thick as the alluvial and marine facies

investigations in the basin, and the offshore study area is spatially limited. While pseudo logs do not fully capture the stratigraphic complexity, they effectively represent the proportion of permeable and impermeable rock types that function as aquifers or confining units. This makes them suitable for constructing a regional hydrogeological model of the offshore facies.

Modeling

Despite the substantial amount of geological information available, its distribution across the study area is highly uneven. This limitation inevitably affects the modeling results. However, it is important to address this issue and provide the most accurate geological reconstruction possible with the available data. To achieve this, a multi-approach modeling method was employed. In the modeling phase, four different three-dimensional models were developed: a geostatistical model (GS model), a lithostratigraphic data interpolation model (LSI model), a trend model of aquifers geometries (TR model), and a cyclothems base geometries model (CB model). Table 1 summarizes the key aspects of each model. In all models, the upper boundary corresponds to the topography, while the cyclothems sequence base defines the lower boundary. The GS and LSI models were built with Petrel (provided by Schlumberger) and Leapfrog GEO (provided

Table 1 Key aspects of the developed models

Model	Model objective	Input data	Methodology	Accuracy	Limitations
GS	Permeable facies distribution	Training set (lithological information)	Geostatistics	86%	Non-unique model result
LSI	Permeable facies distribution	Training set (lithological information)	Interpolation	82%	Geometrical constraint required
TR	Exploited aquifers geometries	Training set (geometrical information)	Clustering and interpolation	-	Large dataset required and challenging clusterization
CB	Cyclothems geometries	Literature and newly interpreted borehole logs and stratigraphies	Interpolation	-	Few data available

GS Geostatistical model, *LSI* Lithostratigraphic data interpolation model; *TR* Trend model of aquifers geometries; *CB* Cyclothems base geometries modeling

by Seequent), respectively, and define the distribution of lithological facies within the study volume. This dual approach was chosen to compare how different methodologies capture lithological heterogeneity based on the same input data. The TR and CB models, both built with Leapfrog GEO, are three-dimensional models of the surfaces that approximate the average geometric trend of the main exploited aquifers (TR model) and cyclothems-related cyclostratigraphy (CB model). The GS, LSI, and TR models use the same input borehole dataset, while the CB model is based on data from previous studies and new interpretations of cyclothem bases. The dataset, used for GS, LSI, and TR models was split into a training set, which is used to build the models, and a testing set, employed to assess their accuracy. The training set consists of the lithostratigraphic dataset, the stratigraphy of pseudo-wells, and 70% of the screen dataset. The training set was edited to exclude lithostratigraphic layers with a thickness greater than 50 m from modeling. This data selection process was implemented differently for the high plain (HP) and low plain (LP) settings since the literature indicates that the former is characterised by greater lithological uniformity and more limited clay-rich horizons than the latter (Zini et al. 2023). In the HP, silty/clay layers exceeding 50 m were discarded from the modeling, whereas in the LP, no lithofacies distinction on layers exceeding 50 m was made. This approach is supported not only by the general understanding of the region's complex meter-scale stratigraphy, which includes numerous thin lenses and layers, particularly in the LP, but also by the fact that well logs were primarily collected for practical purposes. In many cases, log data provided a broad overview of the depths of the most productive aquifer layers rather than being intended for detailed stratigraphic analysis and, for this reason, feature a lower lithological resolution, i.e., a lower distinction between permeable layers and an undifferentiated matrix or highly mixed deposits (e.g., silty clay mixed with gravel). While these logs confirm the presence of aquifers, the characteristics of the surrounding matrix is often unreliable. As a result, this filtering process is unlikely to remove valuable geological information but instead help reduce the noise, thereby improving the overall reliability of the model. The testing set comprises the remaining 30% of the well screens dataset. The well screens dataset was chosen for accuracy calculations as it is considered to be the most robust due to being unaffected by the drilling objective. The accuracy was computed by determining the ratio of data points in the testing set that fell within the permeable sectors of the model to those that fell outside. For this reason, the model accuracy was calculated exclusively for the GS and LSI models which describe the permeable facies distribution.

Large datasets can have their utility compromised if they are not homogeneously distributed across the target area. In this specific case, the calculation of model accuracy is affected by the distribution of the training and testing set. As the data points are mainly concentrated in the north of the LP (Fig. S1c of the ESM), the modeling and validation processes are more robust in the inland area.

Geostatistical model from lithostratigraphic data (GS)

The GS model is a three-dimensional stochastic model in which lithological spatial patterns are estimated via geostatistical methods. Geostatistical methods have been widely used to obtain realizations of sedimentary facies distributions, which are then assigned hydraulic parameter values for groundwater modeling (Maliva et al. 2015). The facies groups identified in the borehole stratigraphy of the training set range from coarse gravel to fine-grained clay and peat. These were grouped into three main classes based on hydraulic conductivity: gravel (class 3, very high permeability), sand (class 2, medium–high permeability), and fine-mixed facies, including mixed silt/clay and peat (class 1, low permeability). Class 1 was specifically defined to represent low-permeability facies by incorporating fine and fine-grained/mixed sediments. The distribution of facies in the model domain was predicted using the sequential indicator simulation (SIS). SIS is a stochastic modeling technique that relies on variogram parameters derived from borehole data (Pyrcz and Deutsch 2014). Variogram models must be inferred from the experimental variogram and expert judgment based on the conceptual geological model (Fig. 2a) (Deutsch and Journel 1992). Each facies class was

constrained by a directional variogram calculated from the borehole data for two horizontal directions (major and minor) and the vertical direction. The vertical correlation length was determined by calculating experimental variograms in the vertical direction. The variogram model for the horizontal directions was determined after making some assumptions about the direction of maximum correlation (i.e., azimuth of the major axis) based on prior geological knowledge of the region. The variogram analysis revealed high correlation lengths for classes 2 (sand) and 3 (gravel) in two directions (i.e., roughly parallel and perpendicular to the coastline). For sand, the dual direction is explained by the fluvial depositional process in combination with coast parallel beach deposits (e.g., dunes and barriers). In the case of gravel, both correlation directions indicate high-energy fluvial processes. The first direction, transverse to the coastline, reflects fluvial deposition close to the river course or paleochannels. The second direction, parallel to the coastline, reflects grain size sorting due to downstream decreasing energy from the mountain river outlet to the coast. This coast-parallel trend is responsible for the HP and LP grain size differences in the contemporary VFP. The variogram analysis of class 1 (low-permeability) was inconclusive, as it returned high correlation lengths in multiple directions. This is likely due to the fact that class 1 encompasses multiple lithological components despite sharing an expected low permeability and thus be related to different and overlapping depositional processes. The variogram model parallel to the coastline was selected for class 2, and perpendicular to the coastline for classes 1 and 3. This is due to the fact that the deposition of shales and gravel is expected to be predominantly fluvial-related, whereas sands are expected to be mostly marine-related. Table 2 summarizes the main geostatistical parameters for each facies. A spherical variogram model was used to fit the experimental variogram for all classes.

Furthermore, lithological trends in both vertical and horizontal directions have been determined from the borehole data and employed as soft constraints. This was done to capture the geological heterogeneity in the model domain as demonstrated in Thomas et al. (2019). The 3D trend for each facies class is shown in Fig. S2 of the ESM.

Table 2 Main parameter values utilized for GS models provided by Petrel data analysis

Facies class	Correlation length (m)			Azimuth °N (major axis)
	Major axis	Minor axis	Vertical	
1—clay/silt	35,000	33,000	30	−40
2—Sand	30,562	17,064	20	58
3—gravel	30,562	17,064	75	−40

Azimuth values are relative to the local coordinate system in Petrel

SIS allows for the generation of multiple facies model realizations, or scenarios from the stochastic model, that all fit the input data. Therefore, the model accuracy calculation described in the "Modeling" section was used as the selection criteria to determine the best-fitting model. The grid contains 30 layers with an average height of 10 m to capture the vertical heterogeneity of the aquifer units and a cell diameter of 250 m in the horizontal direction.

Lithostratigraphic data interpolation model (LSI)

The LSI model is a three-dimensional deterministic model built via interpolation using Leapfrog GEO software, which relies on borehole data to ascertain the lithological chronology or stratigraphic sequences within the surveyed region. The LSI model aims to depict a permeable layer is hosting the aquifers (phreatic and confined) and the aquitards that separate each confined aquifer from the preceding and succeeding ones. To achieve this, borehole lithostratigraphic layers of the training set were clustered into two main subgroups: low permeability (class 1, silt/clay) and high permeability (class 2, sand/gravel). High permeability refers to materials with a hydraulic conductivity greater than approximately 1 m per day. Furthermore, class 2 layers have been clustered based on the aquifer they belong to, according to Zini et al. (2023). Class 2 layers that lie outside the depth range of the aquifer were discarded. Moreover, the lithology of the drillholes was simplified in the pre-modeling processing phase to highlight regional layers and reduce the impact of lenses and local horizons in the modeling. Particularly, layers less than 3 m thick were merged with the prior or subsequent layer of the borehole under consideration based on the similarity of their hydrogeological characteristics. In the modeling phase, confined aquifers in the LP were modeled as multiple separate volumes enclosing layers belonging to the same aquifer. The phreatic aquifer is described in the literature as being very thick in the HP, and considerably thinner in the LP. However, no quantitative estimates are available. For this reason, it was assumed that the phreatic aquifer spans the entire model depth upstream from the resurgence line (HP). Downstream (LP) thickness was estimated assuming the thickness of the permeable contiguous layers laying from the topographic surface to a maximum of 25 m below ground level. The interpolation is performed using Leapfrog's FastRBF™, which has proven particularly suitable for large datasets and complex geological settings as it can provide the smooth surface of interpolation in a short processing time (Cowan et al. 2002).

Trend model of aquifers geometry (TR)

The TR model is a three-dimensional model based solely on the geometric configuration of the training set (maximum

well depth and screen depth). Stratigraphic information is therefore not considered. This decision was based on the assumption that both maximum well depth and screen depth approximates aquifer depth. When displayed as a point cloud, some regions exhibit notably high point densities. These areas with higher-density information represent potential aquifers. Point clouds were manually interpreted and clustered. The clusters were then converted to interpolation surfaces to approximate the geometry of the base of each aquifer. The interpreted points are not uniformly spread over the study area, they are mainly located in the northern part of the LP. To avoid distortion of the geometry of the surfaces implied by the extrapolation over the entire study area, the interpolation surfaces are limited to the area where the information is available. The interpolation is carried out separately for each point cluster. This model development was possible due to the large quantity of data available in the research region and shed light on the advantages of dealing with such large datasets.

Cyclothems base geometries modeling (CB)

The CB model is a three-dimensional representation of the geometries and the thickness of the cyclothems in the study area. It is a simplified representation of the cyclostratigraphy related to the sea level fluctuations dominant frequency since MPT. The interfaces between the cyclothems have been correlated using literature data and newly interpreted borehole stratigraphy. The interpretation and correlation of borehole stratigraphies was guided by the occurrence of bioclasts, such as shell fragments, leaves and other vegetal traces, especially in the eastern part of the study area. Cyclothems were identified in the stratigraphic records of seven boreholes: Azzano Decimo, Pramaggiore, Torre di Mosto, R1, R2, R3, and R4 (Fig. 2a). Overall, cyclothem 1 was identified in 22 boreholes, while cyclothem 5, the least represented, was found to be present in 12 boreholes (see "Cyclothems" section).

To address the challenges described in "Trend model of aquifers geometry (TR)" section, the interpolation was limited to the area with the highest data density. The outcomes of this process were four surfaces representing the base of each cyclothem. The base of the 5th cycle corresponds to the bottom of the model.

Results

Model results

The GS model results are displayed in Fig. 4. The accuracy evaluation of this model was performed across 30 realizations to increase the reliability of the error estimation. Among these, an average accuracy of 85.6% was found, with the highest accuracy of 88.7% achieved in the most favorable scenario. The primary factors determining the optimal model included the model accuracy and the geological knowledge of the study region. The model with the second highest accuracy (88.1%) was selected and shown in all figures, as the model with the highest accuracy predicted an unrealistic thickness of class 1 in the coastal area and offshore. This model was constrained by variogram properties summarized in Table 2, which resulted from the experimental variogram analysis and geological knowledge of the depositional environment. The directional variograms of the three facies classes (class 1: silt/clay, class 2: sand, class 3: gravel) highlighted the nonuniqueness of the main azimuth directions (see the "Geostatistical model from lithostratigraphic data (GS)" section). When testing different azimuths for the direction of maximum correlation in geostatistical variogram analysis, the presence of more than one direction with very high values can be attributed to several factors, including anisotropy, complex geological structures, and the overlapping influences of different geological processes (Chiles and Delfiner 2012). Considering the geological setting, the subsurface facies anisotropy caused by the interaction of multiple geological processes is probably the most likely explanation.

The LSI model results are displayed in Fig. 5. The accuracy evaluation of this model is estimated at 82%. High uncertainties are expected to be present in the northern part of the model as it is unclear where and if aquitards pinch out.

The TR model construction phases are displayed in Fig. 6. The interpretation highlights six clusters from the topography to the bottom of the model. The shallowest cluster corresponds to the water table (Ph), while the five deeper clusters correspond to confined aquifers (A1, A2, A3, A4, A5). A5 lies at a depth greater than the base of the model. The model highlights a southern azimuth direction for all clusters and an increasing vertical distance and a surface dip that decreases from the shallowest to the deepest cluster. A multidirectional interpretation of the point cloud is displayed in Fig. S2 of the ESM.

The CB model results are shown in Figs. 7, 8, and 9 as cross-correlation panels and correlated with the GS and LSI models in Figs. 4 and 5. There is a general trend in cyclothems becoming shallower and thinner in the northern and eastern directions. The thinning in the eastern direction is due to different subsidence rates within the region, up to 60–70 mm a^{-1} north of Bologna (Carminati and Martinelli 2002) and 5–2 mm a^{-1} near Aquileia in the eastern sector of the VFP (Da Lio and Tosi 2018). The thinning in the northern direction is due to a topographic change into the steeper, gravelly deposits of the High Plain of the Alpine Piedmont. Figures 8 and 9 outline the closure of the uppermost cyclothem in the northern direction

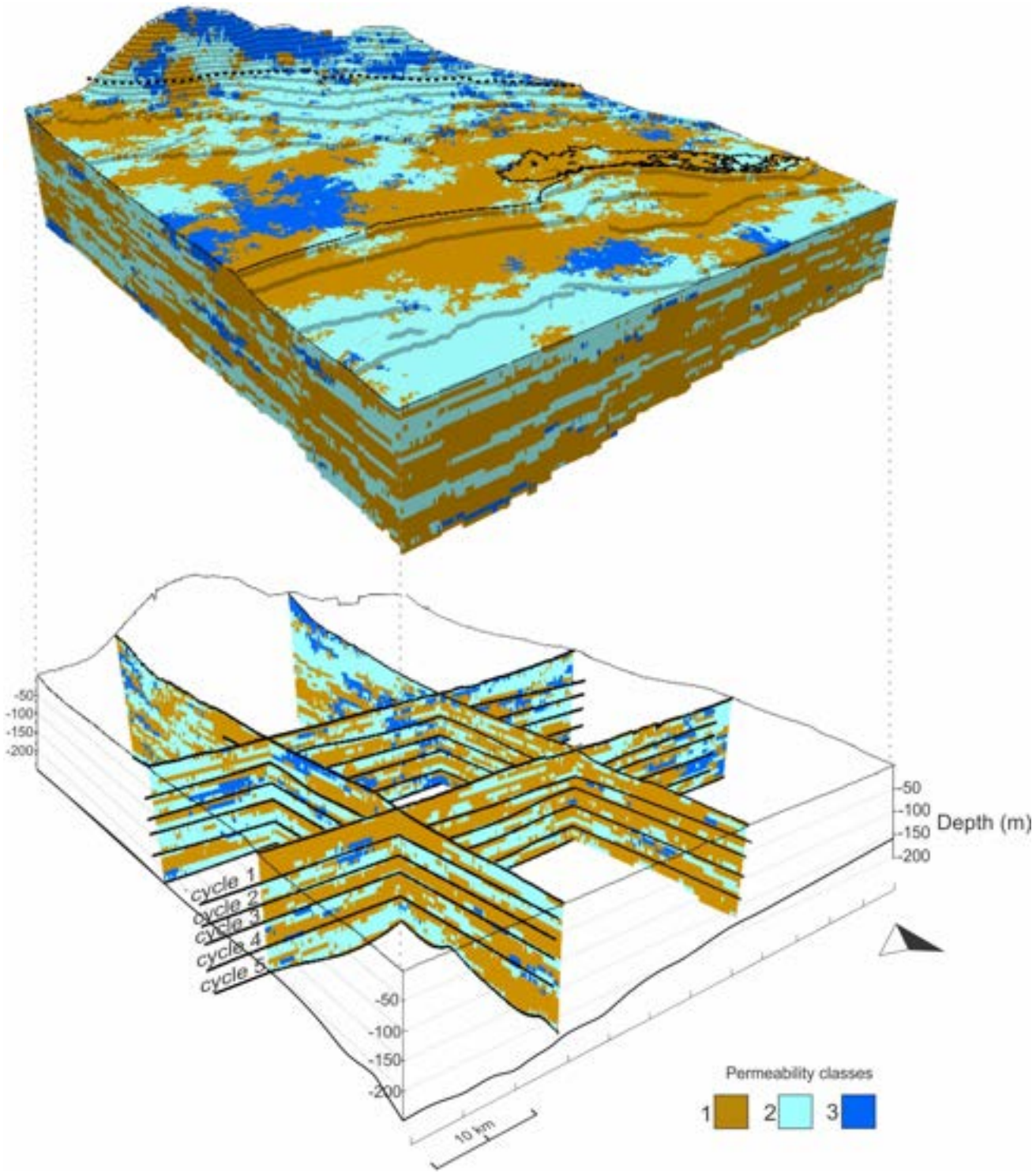

Fig. 4 GS model, computed and displayed by using Petrel, correlation with CB model (cycle 1 to 5). Class 1: silt/clay; Class 2: sand; Class 3: gravel. The solid black line is the coastline, and the blue dashed line is the resurgence line

because the sedimentary fill of the basin has constrained the northward onshore extent of transgressions over time (Amadori et al. 2020). As a result, the northern part of the study area, above the last interglacial maximum flooding surface (Fontana et al. 2010), did not record the last cyclothem.

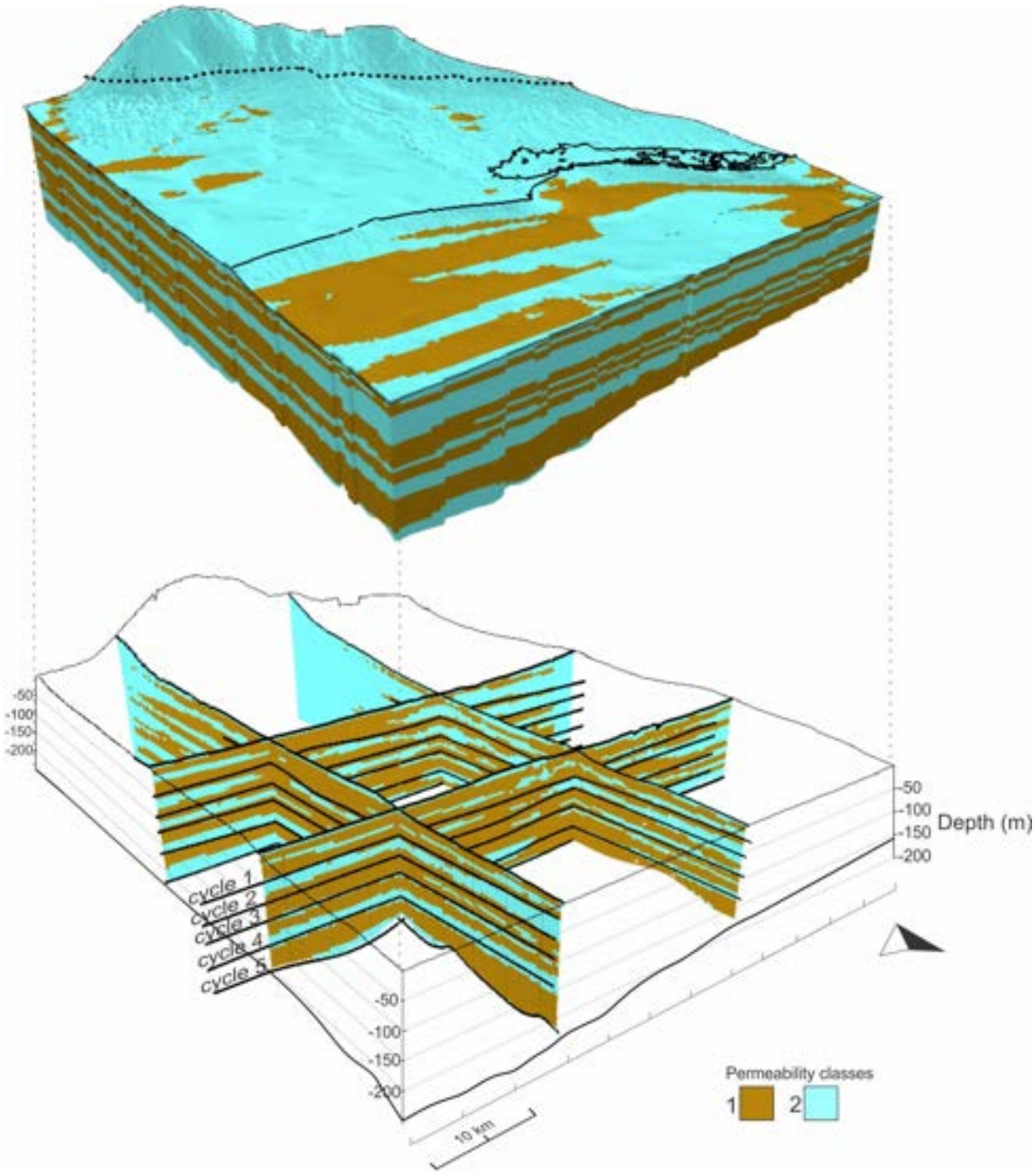

Fig. 5 LSI model, computed with Leapfrog GEO and displayed using Petrel, correlation with CB model (cycle 1 to 5). Class 1: low permeability lithologies; Class 2: high permeability lithologies. The *solid black line* is the coastline, and the *dashed blue line* is the resurgence line

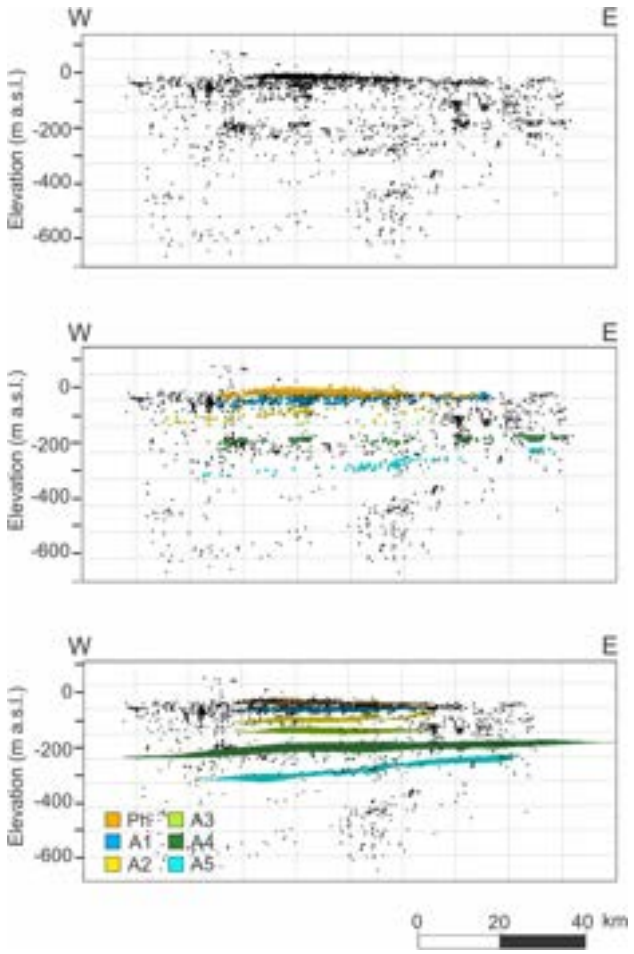

Fig. 6 Clustering and interpolation for the TR model. This figure depicts the horizon-aligned view of the well screens point cloud (top), the subsequent clustering (middle) and interpolation of clusters to derive surfaces representing the geometric trend of each aquifer (bottom). Ph, A1 A2, A3, A4, A5 represents, respectively, the phreatic and five shallower confined aquifers. It is important to acknowledge the challenge of visualizing clusters due to the differential slopes they exhibit. For a more in-depth understanding of point cloud interpretation, refer to Fig. S2 of the ESM

Preliminary estimates of offshore freshwater volumes

Onshore, the compiled database reveals that freshwater-saturated sediments extend hundreds of meters below the ground level, including the coastal area (Fig. S3a of the ESM). This study provides an initial effort to determine their potential offshore extension and geometry. Currently, saline intrusion in the region has been identified in the shallower phreatic aquifer (Pezzatta et al. 2011; Zavagno et al. 2015). ARPA FVG monitors the salinity of confined aquifers primarily through periodic sampling and analysis of a network of confined groundwater wells. Additionally, information on salinity was inferred from the water quality monitoring of licensed water wells, which are mainly utilized for drinking, agricultural, and commercial purposes. Since no salinity issues have been reported so far (Corradin 2025), this suggests that the freshwater–saltwater interface of confined aquifers is likely to be located offshore.

Despite limited information, the offshore well Assunta 1, located nearby the study area, is the only offshore well that features information on pore water salinity, highlighting freshwater (salinity lower than 1%) in the upper 340 m and from 702 to 908 m bsl. Although groundwater modeling will be the next critical step for a comprehensive quantitative evaluation, two preliminary estimates of the volume of offshore freshwater stored in permeable layers are provided, using both the GS and LSI models (Fig. S3b,c of the ESM). The first scenario considers freshwater-saturated sediments up to 3 km from the shore, which is the distance of the Assunta 1 well from the coastline (Fig. S3b of the ESM), while the second scenario predicts freshwater-saturated sediments in the entire offshore modeled area (Fig. S3c of the ESM). These calculations assume a constant effective porosity of 30% for sand facies and 40% for gravel facies (Wolff 1982) in the three-class GS model and 30% as the permeable facies in the two-class LSI model. The assumption of 30% effective porosity for sand in the GS model is based on the presence of unconsolidated sediments with no cemented layers or sandstones. Given that the study volume extends to a maximum depth of 260 m, significant porosity reduction due to compaction is unlikely. The derived volumes of the two scenarios are 4.4 and 23.2 km^3, respectively, for the GS model, while 3.8 and 24.9 km^3 for the LSI model.

Discussion

Aquifer modeling

In the hydrogeological investigation of the VFP aquifer system and potential OFG in the NAB, a key step is to develop a groundwater model. This model will help assess the sustainability of onshore water extraction and estimate offshore-directed groundwater fluxes. It will be built upon the geological framework of the VFP and NAB, which was established in this study, where the multi-modeling approach provides an understanding of the distribution of aquifers in terms of the lithology, facies, and stratigraphy of their host sediments (GS, LSI, cyclothem models), as well as the depth of water capture (TR model). These models were built upon several assumptions due to uneven data distribution. The differences and limitations of the four models are discussed below.

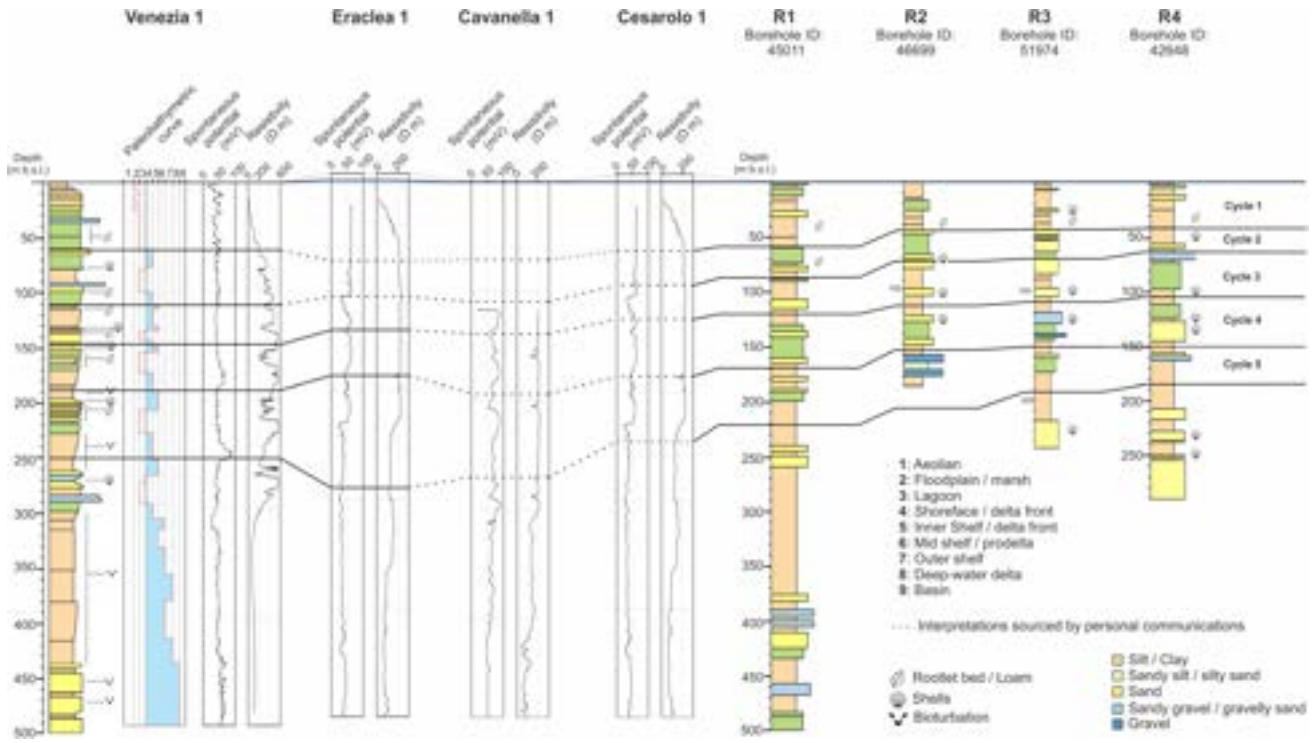

Fig. 7 Along-coast cyclothems correlation panel. This correlation panel counts eight onshore boreholes. Venezia 1 (borehole stratigraphy, paleobathymetric curve, interpretation for five cyclothems), Eraclea 1 (three deepest cyclothems) are sourced from Amadori et al. 2020. Eraclea 1 (two shallower cycles), Cavanella 1, and Cesarolo 1 interpretation of cyclothems are sourced by M. Ghielmi (ENI E&P, personal communication, 2023). R1, R2, R3, and R4 belong to the onshore borehole dataset and have been newly interpreted for cyclothems. The distance between boreholes is not scaled

Facies model (GS and LSI models)

The GS and LSI models are both facies distribution models which, despite some differences, provide a comparable result and achieve good accuracy. Both models show alternating layers of permeable and non-permeable classes with the following differences: geological validity, aquifer slope and interconnectivity & aquifer geometry are supposed to be different points of the same list. they should have the same style, preferably the style of 'aquifer geometry' list point.

Geological validity

The LSI model, based on stratigraphic log interpolation, results in a layer-cake appearance. However, this interpolation likely oversimplifies the geological complexity, producing a model that is useful but not fully representative of the actual subsurface geology. In comparison, the GS model yields a patchier spatial distribution of lithological classes, which produces a less spatially continuous result. A patchy model geometry is a common feature of geostatistical methods such as SIS, which rely on traditional variogram statistics where only the correlation between two points is considered (Webster and Oliver 2007). A more discontinuous facies distribution may better reflect geological reality, particularly in settings where fluvial, glacial, and marine processes interact.

Aquifer slope and interconnectivity

The GS model better captures geological and stratigraphic trends, such as the vertical interconnectivity of permeable areas and the stratigraphic dip.

Aquifer geometry

The GS model better reflects the uncertainty of the potential landward extent of the deeper aquifers, which is not comprehensively addressed in the existing literature. This model indicates that the artesian aquifers could extend further northward despite a significant decrease in clay content in the HP, and thus the discontinuity of aquitards. On the other hand, the LSI model restricts the presence of artesian aquifers in the LP as suggested by the literature and thus in the proximity of the resurgence line.

In summary, the GS model is better suited to an analysis where there is limited data control or where alternative

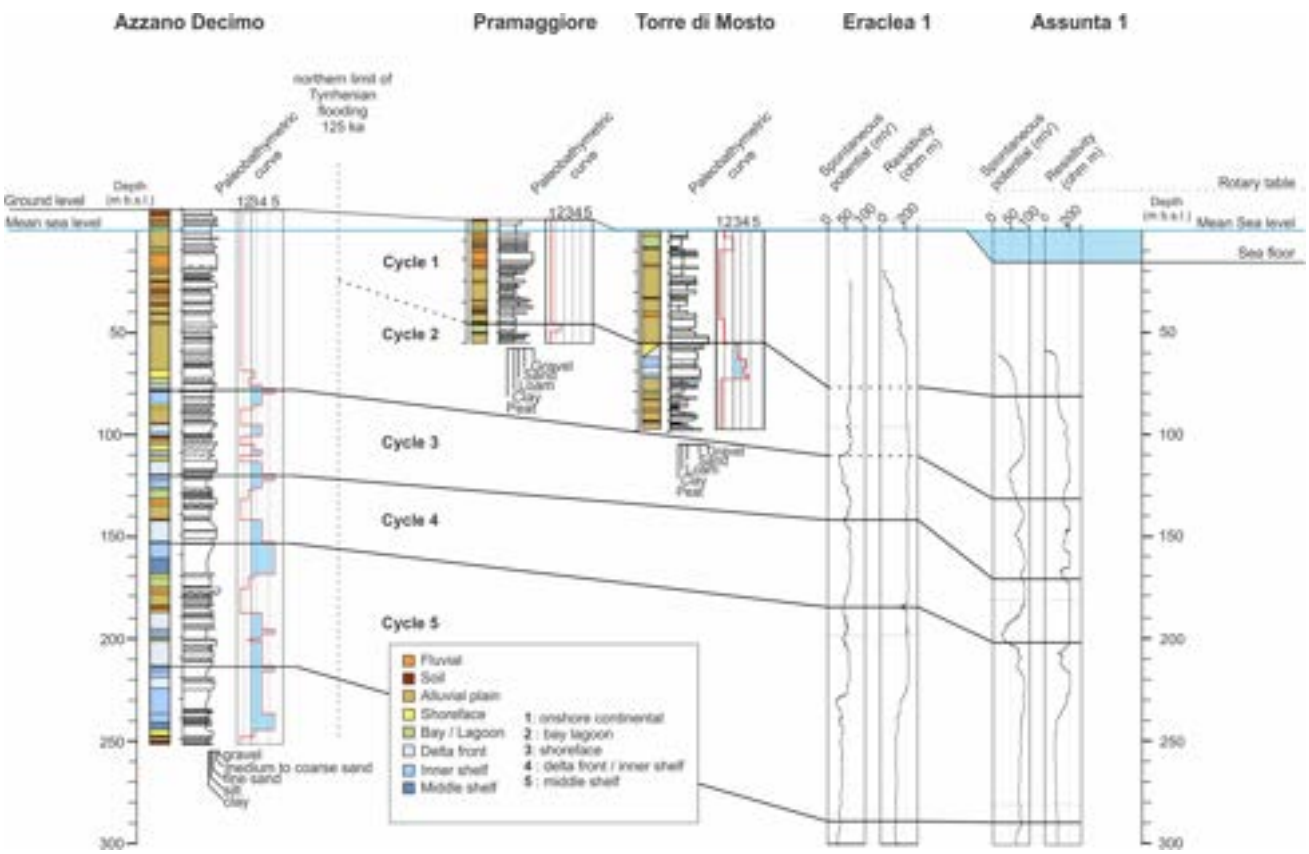

Fig. 8 Onshore–Offshore correlation panel. This correlation panel counts four onshore and one offshore borehole. Assunta 1 (five cycles) and Eraclea 1 (three deepest cycles) are sourced from Amadori et al. (2020). Eraclea 1 (two shallower cycles) is sourced by M. Ghielmi (ENI E&P, personal communication, 2023). Borehole stratigraphy, paleobathymetric curve, and depositional environment analysis of the Azzano Decimo borehole are sourced from Zanferrari et al. (2008) and of Pramaggiore and Torre di Mosto boreholes are sourced from Fontana et al. (2010; 2012). Azzano Decimo, Pramaggiore, and Torre di Mosto correlation is modified after Fontana et al. (2010) and newly interpreted for cyclothems. The distance between boreholes and the location of the northern limit of Tyrrhenian flooding is not scaled

hypotheses to the existing literature are to be tested, while the LSI better represents the distribution of host sediments of the aquifer based on pre-existing literature data. Despite both models demonstrating high accuracy, the geostatistical model is considered more geologically realistic and better represents the Venetian-Friulian Plain and NAB.

Model of exploited aquifers (TR model)

The TR model was developed through manual spatial clusterization and successive interpolation of higher-density point cloud areas displaying a roughly planar subhorizontal geometry that resembled a stratification (Fig. 5, Fig. S4 of the ESM). Thus, the robustness of this methodology is proportional to the magnitude of the input dataset. In this study, the vast amount of data available makes the model very robust for a regional representation. However, locally, a lack of data due to either the intrinsic absence of an aquifer itself or the lack of data for unknown reasons, was observed. As an example, in the deeper part of the model, the absence of aquifers in large areas could also be explained by the absence of boreholes, for example, rather than their absence. This is a possible limitation of the model that should be considered when producing a detailed local model.

Correlations between models

Overall, the CB model (cycles 1, 2, 3, 4, 5) correlates best with the LSI model, which is due to the good fit between the base of cyclothems and the interfaces between permeable (below) and impermeable (above) layers.

Figure 10 displays the correlation between the LSI model, the CB model and the TR model (Ph, A1, A2, A3, A4). There is a good correlation between A2 and A3 surfaces and cycles 1 and 2 of the CB model, matching the basal surface of each cycle. The correlation of A1 with cyclothems is unclear. A1 lies between 20 and 35 m bsl and matches the top of a high permeability layer of the LSI model that is

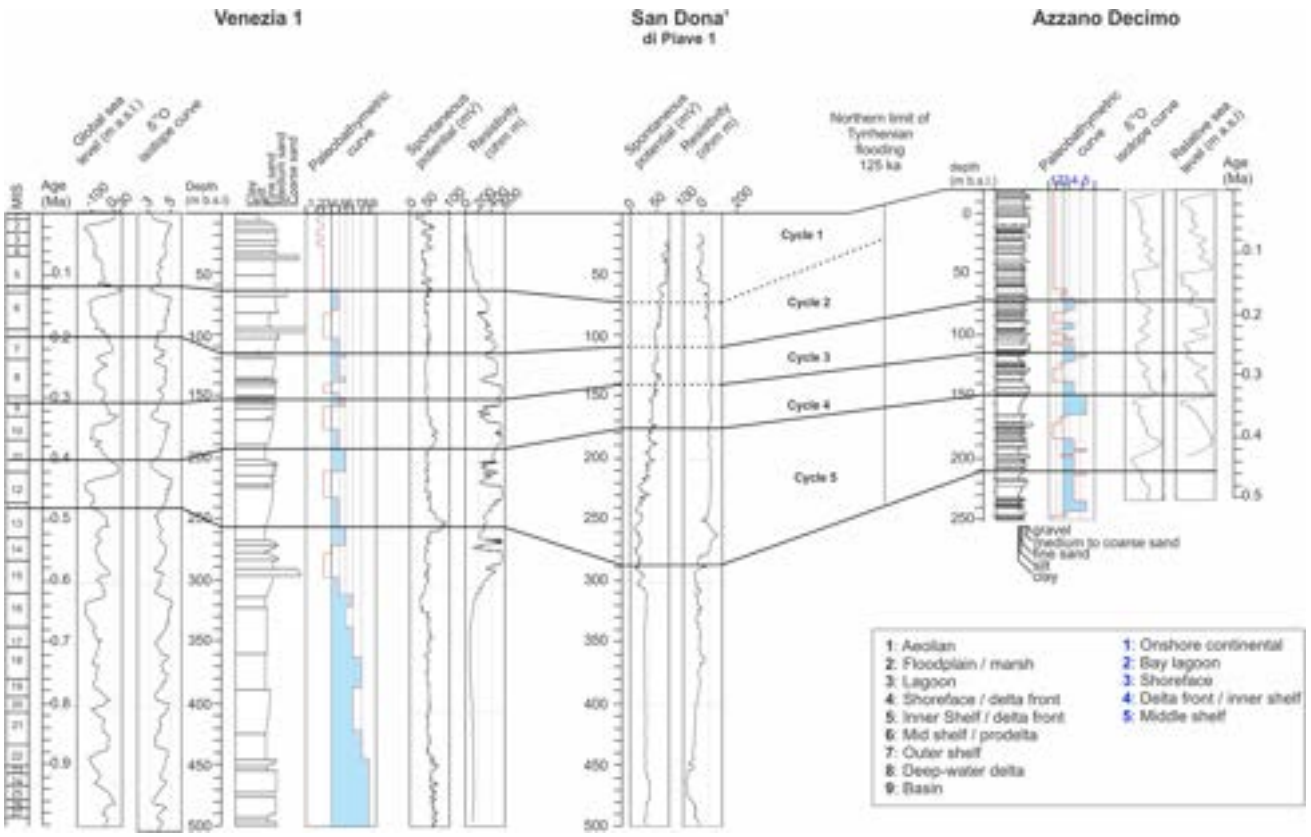

Fig. 9 Venezia 1, San Dona', and Azzano Decimo well log correlation panel. Venezia 1 provides stratigraphy, interpretation of five cyclothems, paleobathymetric curve, MIS correlation, isotope curve, and the global sea level curve), San Donà di Piave 1 (two deepest cycles) are sourced from Amadori et al. (2020). Three shallower cycles of San Donà di Piave 1 are sourced by M. Ghielmi (ENI E&P, personal communication, 2023). Azzano Decimo is modified after Zanferrari et al. (2008) and newly interpreted for cyclothems. The distance between boreholes and the location of the northern limit of Tyrrhenian flooding is not scaled

missing in the central part of the study area. Its depth is coincident with a gravelly sand horizon of the Azzano Decimo borehole deposited in a continental environment (Zanferrari et al. 2008). Radiocarbon dating samples from the bottom of this layer in the Azzano Decimo borehole, which yielded an age of 23.4 ± 0.3 ka, suggest deposition during the Last Glacial Maximum. It is inferred that the aquifer associated with this horizon is a depositional relict of the progradation of the HP and resurgence line during the last glacial period. With the exception of the northern part, A4 in Fig. 10a exhibits a good correlation with the lower portion of cyclothem 4, while the correlation in Fig. 10b is notably weaker. Additionally, A4 generally has a steeper slope compared to the other TR model surfaces in the northern sector of the model. This is consistent with the expected tilting of older deposits in an actively subsiding basin. The separation between A3 and A4 is greater than in the other surfaces. In this depth range, Zini et al. (2023) suggest the presence of a discontinuous aquifer, which is locally divided into two minor aquifers and is absent in the western part of the study area. Furthermore, as mentioned in the "Cyclothems" section, cyclothem 3 has been found to represent the sedimentological record of two minor astronomical cycles rather than one 100,000 year cycle. It is suggested that, within this depth range, eventually the aquifer may either become too thin to be captured with the current model resolution, or it may be locally absent in the region. The correlation identified suggests a connection between layers containing aquifers and cyclothems, with the exception of the shallower aquifer (A1 of TR model). Moreover, the sedimentary record of each cyclothem encompasses a layer with high permeability, serving as a reservoir for freshwater. This outcome emphasizes the potential for predicting the presence of the aquifer based on cyclothem distribution. The models indicated that the aquifers, apart from sedimentary lenses and localized horizons, are mainly independent and probably have limited water exchange, as already noted by Zini et al. (2023).

Aquifer genesis

The marine and coastal component of the depositional processes that built the VFP decreases northward because of

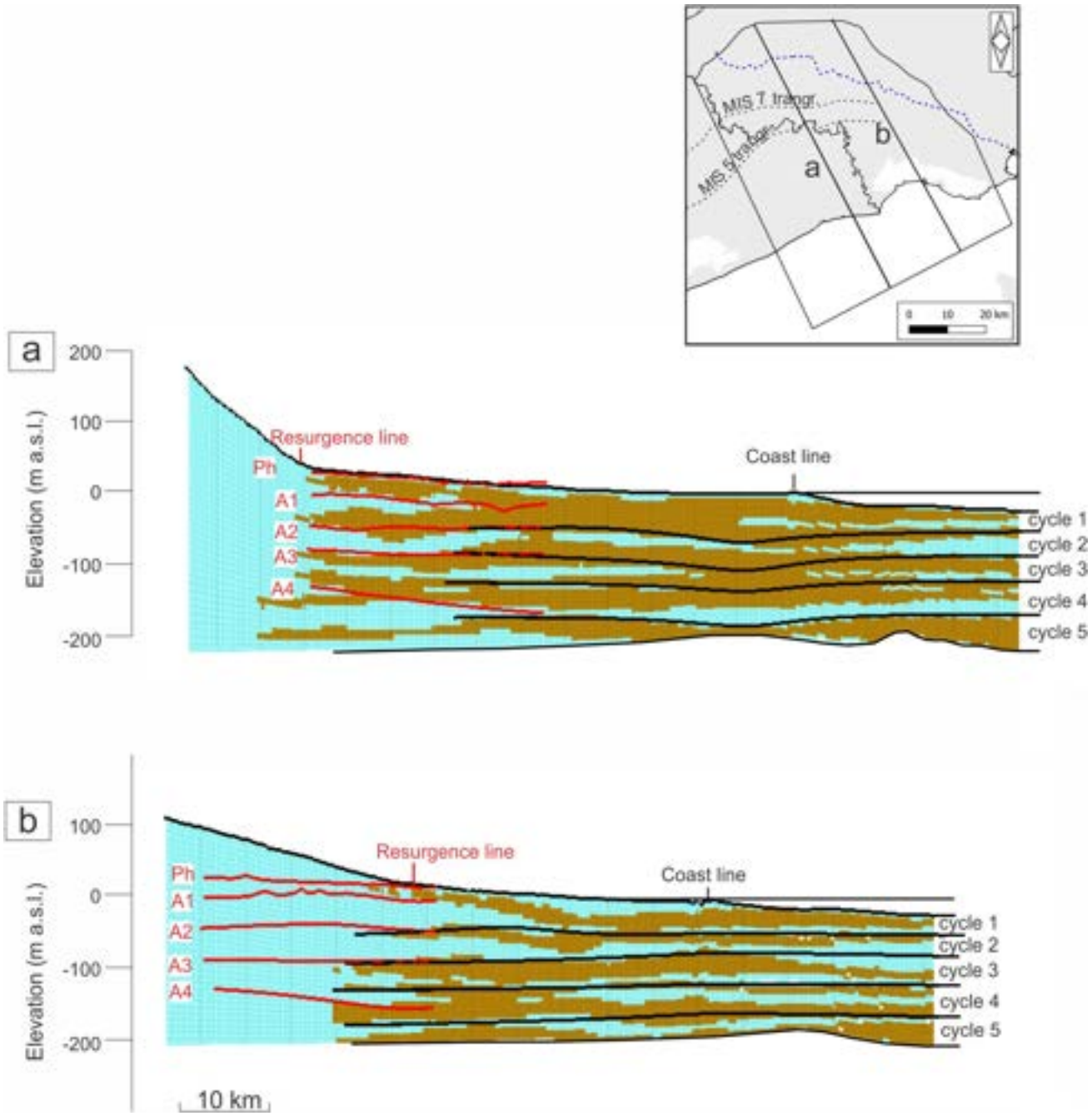

Fig. 10 LSI, CB, and TR model correlation. Sections of the LSI model correlated with the CB model (cycles 1 to 5) and the TR model (PH and A1 to A4). Ph represents the phreatic aquifer. A5 is not represented since it lies at a depth greater than the bottom of the model. The map displays the study area, the resurgence spring belt (*blue dashed line*), LSI model sections (**a** and **b**), and MIS 5 and 7 transgressions (modified after Marcolla et al. 2021)

the progressive FVP progradation toward the NAB (Amadori et al. 2020). The maximum flooding surface (MFS) of the last two interglacial periods is partially mapped in the subsurface of the study area (Marcolla et al. 2021). Near the Tagliamento River, the MIS 7 MFS is located 25 km from the present-day coastline, while the MIS 5 MFS is 20 km from the coastline (Fig. 2, 11). The MFS in the eastern part of the study area are likely positioned farther basinward.

The gathered evidence suggests that the confined layered aquifers of the VFP have a genesis linked to the combined effect of deposition in a continental environment (fluvial/alluvial) and transition environment (coastal/shoreface). Whereas north of the MFS, fluvial processes are solely

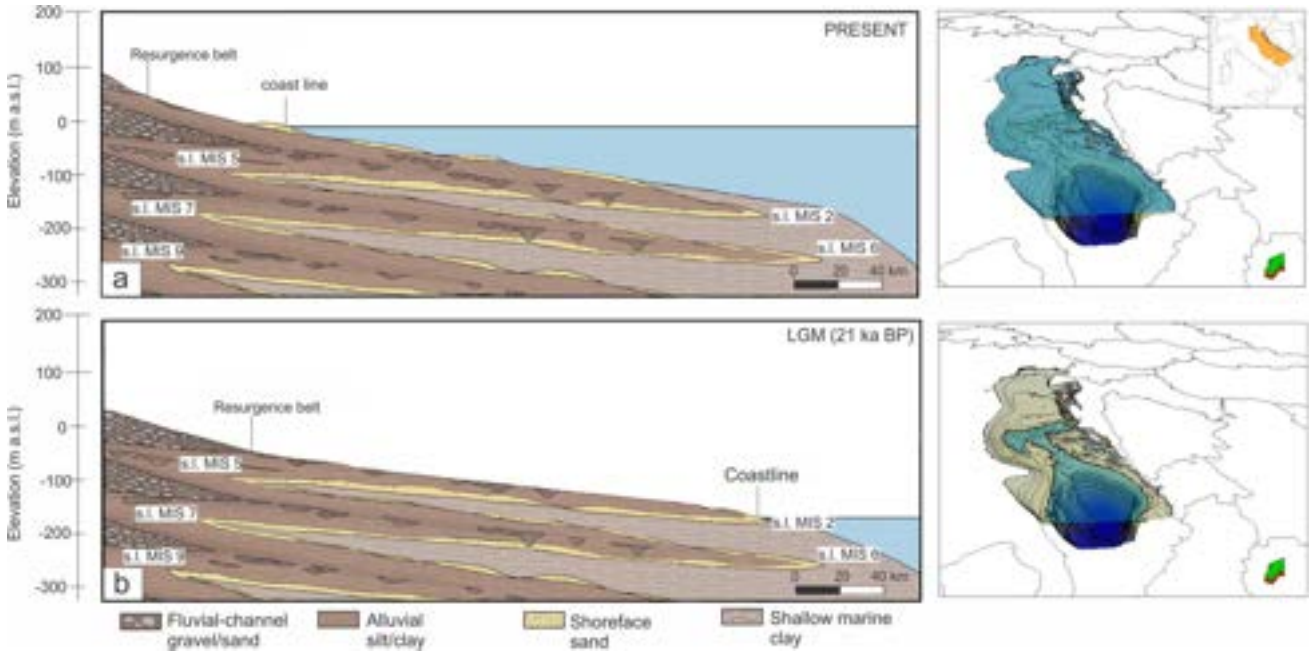

Fig. 11 Conceptual representation of the expected stratigraphy driven by Pliocene to Quaternary glacio-eustatic fluctuations in the NAB. (**a**) (left) Represents the current coastline and resurgence line locations and the associated deposits; and (right) the 3D bathymetric model of the modern NAB totally submerged by present sea level. (**b**) (left) depicts the location of the southern coastline during the LGM; and (right) the aerial exposure of the NAB during the same period (Vai et al. 2004). The vertical and horizontal scales are magnified by a factor of 7500 and 1.5 million, respectively

responsible for aquifer-bearing formation deposition. It is proposed that south of each past MFS, the depositional environment, though mixed, is predominantly marine. More specifically, it is suggested that in the coastal area of the VFP aquifers originated as river-borne sediments, but they were later reworked and sorted by the action of coastal waves, winds, and currents. The relatively larger component of marine/coastal sediments in the genesis of the VFP aquifers is a step forward with respect to the current understanding (Zini et al. 2023), where evidence supporting this hypothesis is presented below:

(a) Lithological composition of aquifers. Aquifers hosting sediments are, in the LP, mainly moderately to well-sorted sand and rarely gravelly sediments. Well-sorted sand deposits in the region are typical of coastal and beach systems (Fig. S1a of the ESM) and are probably the result of sediment sorting by wind, waves and currents (e.g., Brambati et al. 1983);
(b) Regional extent of the permeable deposits hosting the aquifers. Despite showing some discontinuities, aquifers span the entire study area. However, this lateral extension does not apply to the four modern alluvial megafans (Tagliamento, Corno, Cormor and Isonzo rivers) that coexist in the study area, thus excluding a fluvial genesis (Fontana et al. 2008);
(c) Sand lithological facies hosting the aquifers exhibit a coast-parallel anisotropy, which is highlighted by the class 2 variogram analysis of the GS model (see the "Model of exploited aquifers (TR model)" section);
(d) A narrow relict coastal sandy deposit spanning the entire SW-NE extent of the study area for approximately 440 km^2, has been recognized in the offshore area (see "The Northern Adriatic Basin (NAB)" section) (Fig. S1a of the ESM) (e.g., Brambati et al. 1983);
(e) 252 stratigraphic records from boreholes in the study area or nearby show evidence of Middle to Late Pleistocene seashells in sandy and silty/clay layers, including bivalves and ostracods, suggesting the widespread presence of marine/coastal deposits (Fig. S5 of the ESM);
(f) Middle to Late Pleistocene marine sedimentary facies have been identified up to 35 km north of the coast in the Azzano Decimo suggesting that sea level fluctuations influenced a large part of the study area (Zanferrari et al. 2008);
(g) The consistent vertical spacing of the modeled aquifers suggests repetitive depositional processes occurring at regular intervals. This pattern reflects a cyclic repetition of sedimentation within a relatively stable basin setting, where sediment input originated from consistent sources, and sea-level fluctuations remained comparable over time.

Further investigation is needed to determine the extent to which fluvial and coastal aquifer systems are interconnected and whether they interact hydraulically.

The potential of the NAB for hosting offshore groundwater aquifers

Literature discussing the investigation of cyclothems geometries in the NAB is still scarce and mainly focused on the northern and western margins, as described in the "*Cyclothems*" section, mainly due to the lack of available data in this area. In this paper, the onshore–offshore cyclothems correlation has been extended northward and eastward allowing to link sandy groundwater bearing formation onshore to the Pliocene to Quaternary sea level cyclicity. It was found that onshore aquifers are laterally interconnected for kilometers both northward and along the coast. Despite that a broader areal analysis is outside the scope of this study, after these findings, some hypotheses might be formulated, assuming a comparable stratigraphic framework in the siliciclastic region of the NAB, which has experienced consistent geological processes and depositional history. Cyclothems sequence is thicker and mostly continuous offshore with no evidence of major erosion or non-deposition (Amadori et al. 2020; Zecchin et al. 2022), although it shows minor erosional surfaces such as ravinement surfaces or subaerial erosion (e.g., Zanferrari et al. 2008; Massari et al. 2004). For this reason, each cyclothem is expected to exhibit a seaward-directed, wedge-shaped sedimentary sequence, counting two main coastal sandy deposits, associated with regression and transgression, respectively, and alternating with silty/clay marine and alluvial sediments. Within this broader depositional framework, fluvial gravel deposits, such as fan and channel systems, are superimposed, contributing to local discontinuities and forming localized deposits and horizons. A conceptual 2D representation of the expected stratigraphy of the NAB is displayed in Fig. 11. This geological framework closely resembles the onshore reconstruction model proposed by Amorosi et al. (2016) and is supported by the facies analysis of the Venezia 1 well (Massari et al. 2004; Amadori et al. 2020), where the stratigraphic log highlights two coastal deposits, one thinner and sea level transgression related and the other thicker and related to regression.

Therefore, this study suggests that, given the sea level cyclicity of the Middle Pleistocene to Holocene interval throughout the Adriatic Basin, it is highly possible that coastal deposits are likely present in most of the northern and central Adriatic Basin. For this reason we also suggest that it is reasonable to expect also onshore aquifers to extend basinward in the Adriatic Shelf.

Further investigation is warranted to assess thickness, preservation, and lateral connectivity of these deposits. Additionally, determining whether these deposits are saturated with fresh, freshened, or saltwater remains an open question. The next step is to develop a groundwater numerical model within the modeled geological framework to investigate involved Water budgets and salinity dynamics. Meanwhile, the preliminary estimates suggest that OFG volume in the study area ranges from 3.8 km^3 in the most conservative scenario to nearly 25 km^3 in the most favorable case. It is also suggested that freshwater emplacement mechanisms in this area are likely to be related to onshore–offshore active recharge, or to recharge during sea level lowstands.

Conclusions

The geometry, extent, and volume of the confined aquifers in the lower Venetian-Friulian plain and the northern Adriatic Sea were reconstructed using three-dimensional geological modeling. The results show that the aquifers are present as discontinuous sand bodies that are distributed within a complex matrix of silts and clays with lower-permeability and that there is a high likelihood of onshore–offshore connectivity of the VFP aquifer system. The presence of sand bodies can be attributed to buried coastal deposits formed by marine reworking and sorting of fluvial sediments during sea level fluctuations since the Middle Pleistocene Transition (MPT). This conclusion is supported by several key observations, including lithological characteristics, fossil records, onshore marine facies, and the lateral continuity and cyclical patterns indicative of coastal/shallow marine environments. The identification of cyclical deposits extending offshore to the meso-Adriatic deep, coupled with the abundance of well-preserved sand deposits in the region, strongly indicates the potential for the NAB to host offshore freshened groundwater aquifers. This suggests significant promise for further exploration and assessment of these potential resources in the northern Adriatic Basin.

Supplementary Information The online version contains supplementary material available at https://doi.org/10.1007/s10040-025-02952-w.

Acknowledgements We would like to thank the project partner LTA S.p.A. for providing a precious dataset for the modeling. We acknowledge Schlumberger for providing the academic licence for the Petrel® software at the University of Trieste, and Seequent for providing the academic license for Leapfrog GEO.

We want to express our sincere gratitude to Manlio Ghielmi, Chiara Amadori, Sara Oberti, Davide Brandolin, Federica Donda, Massimo Zecchin, Annelore Bezzi, and Francesco Treu whose feedback and discussions have been extremely helpful for this paper.

The authors also acknowledge ISPRA (Istituto Superiore per la Protezione e la Ricerca Ambientale), for providing subsurface data from the National Archive of Subsurface Surveys, pursuant to Law 464/84.

Finally, the authors would like to express their sincere gratitude to the reviewers and editors for their valuable insights and constructive feedback, which significantly contributed to enhancing the quality of this work.

Author contribution C Corradin, AT Thomas, A Camerlenghi, L Zini, M Giustiniani, M Busetti, L Foglia, C Bertoni, and A Micallef conceived and planned the study. C Corradin, AT Thomas, C Bertoni and M Giustiniani carried out the data curation, formal analysis, and investigation. AT Thomas and A Micallef planned and implemented the methodology and software development. C Corradin took the lead in writing the original draft and all of the authors contributed to reviewing and editing the manuscript. A Camerlenghi, L Zini, and A Micallef secured funding and resources. All authors provided critical feedback and helped shape the research, analysis, and manuscript.

Funding This study was conducted with the co-financing of the European Union—FSE REACT EU, PON Research and Innovation 2014–2020 and University of Malta. (A.M. was supported by the David and Lucile Packard Foundation); and the PNRR research activities of the consortium iNEST (Interconnected North-East Innovation Ecosystem) funded by the European Union Next-GenerationEU (Piano Nazionale di Ripresa e Resilienza (PNRR) – Missione 4 Componente 2, Investimento 1.5 – D.D. 1058 23/06/2022, ECS_00000043). Moreover, this study was supported by OGS within the activities BlueSkills: Blue Jobs and Responsible Growth in the Mediterranean funded by the Italian Ministry of University and Research (MUR) and labeled by the Union for the Mediterranean (UfM).

This publication is based upon work from CA21112 – Offshore freshened groundwater: An unconventional water resource in coastal regions? – OFF-SOURCE", supported by COST (European Cooperation in Science and Technology).

The authors would also like to thank the European Commission and MIUR for funding in the frame of the collaborative international consortium RESCUE financed under the 2022 Joint call of the European Partnership 101,060,874 — Water4All."

Availability of data The dataset of regional stratigraphic boreholes used in this study cannot be publicly shared as it is managed by local authorities and contains licensed and citizen-related data. The model resulting from this study (GS, LSI, TR, and CB) is available upon request.

Declarations

Competing interests The authors declare that they have no known competing financial interests or personal relationships that could have appeared to influence the work reported in this paper.

References

ARPA FVG (2018) Studio conoscitivo dei cambiamenti climatici e di alcuni loro impatti in Friuli Venezia Giulia, www.meteo.fvg.it/clima/clima_fvg/03_cambiamenti_climatici/01_REPORT_cambiamenti_climatici_e_impatti_per_il_FVG/impattiCCinFVG_marzo2018.pdf

Amadori C, Ghielmi M, Mancin N, Toscani G (2020) The evolution of a coastal wedge in response to Plio-Pleistocene climate change: the northern Adriatic case. Mar Pet Geol 122:104675. https://doi.org/10.1016/j.marpetgeo.2020.104675

Amorosi A, Maselli V, Trincardi F (2016) Onshore to offshore anatomy of a late Quaternary source-to-sink system (Po Plain-Adriatic Sea, Italy). Earth-Sci Rev 153:212–237. https://doi.org/10.1016/j.earscirev.2015.10.010

Ayeni G, Huck A, De Groot P (2008) Extending reservoir property prediction with pseudo-wells. First Break 26(11)

Brambati A, Ciabatti M, Fanzutti GP, Marabini F, Marocco R (1983) A new sedimentological textural map of the northern and central Adriatic Sea

Brancatelli G, Busetti M, Dal Cin M, Forlin E (2023) Reprocessing the CROP95-M18 vintage multichannel seismic data acquired in the northern Adriatic Sea: the case of high penetration crustal profile recorded in shallow waters. Bull Geophys Oceanography 64(3):213–236. https://doi.org/10.4430/bgo00419

Bresolin M (2013) Late Pleistocene evolution of the low Friulian Plain (NE ITALY). Master's thesis, University of Padua, Padua, Italy

Bronstert A, Niehoff D, Schiffler GR (2023) Modelling infiltration and infiltration excess: the importance of fast and local processes. Hydrol Process 37(4):e14875

Busetti M, Volpi V, Nicolich R, Barison E, Romeo R, Baradello L, Brancatelli G, Giustiniani M, Marchi M, Zanolla C, Wardell N, Nieto D, Ramella R (2010) Dinaric tectonic features in the Gulf of Trieste (northern Adriatic Sea). Boll Geofis Teor Appl 51(2–3):117–128

Campo B, Amorosi A, Vaiani SC (2017) Sequence stratigraphy and late quaternary paleoenvironmental evolution of the Northern Adriatic coastal plain (Italy). Palaeogeogr Palaeoclimatol Palaeoecol 466:265–278. https://doi.org/10.1016/j.palaeo.2016.11.016

Campo B, Pellegrini C, Sammartino I, Trincardi F, Amorosi A (2024) New perspectives on offshore groundwater exploration through integrated sequence-stratigraphy and source-to-sink analysis: insights from the late Quaternary succession of the western Central Adriatic system, Italy. Earth-Sci Rev. https://doi.org/10.1016/j.earscirev.2024.104880

Canter LW (1982) Groundwater quality management. J AWWA 74:521–527. https://doi.org/10.1002/j.1551-8833.1982.tb04995.x

Carminati E, Martinelli G (2002) Subsidence rates in the Po Plain, northern Italy: the relative impact of natural and anthropogenic causation. Eng Geol 66:241–255. https://doi.org/10.1016/S0013-7952(02)00031-5

Carminati E, Doglioni C, Scrocca D (2003) Apennines subduction-related subsidence of Venice (Italy). Geophys Res Lett 30:2003GL017001. https://doi.org/10.1029/2003GL017001

Carton A, Bondesan A, Fontana A, Meneghel M, Miola A, Mozzi P, Primon S, Surian N (2009) Geomorphological evolution and sediment transfer in the Piave River system (northeastern Italy) since the last glacial maximum. Geomorphologie 15(3):155–174. https://doi.org/10.4000/geomorphologie.7639

Cattaneo A, Trincardi F, Asioli A, Correggiari A (2007) The Western Adriatic shelf clinoform: energy-limited bottomset. Cont Shelf Res 27(3–4):506–525

Chiles JP, Delfiner P (2012) Geostatistics modeling spatial uncertainty. Wiley, Hoboken N.J

Colantoni P, Gallignani P, Lenaz R (1979) Late Pleistocene and Holocene evolution of the North Adriatic continental shelf (Italy). Mar Geol 33:M41–M50. https://doi.org/10.1016/0025-3227(79)90130-0

Connolly PA, Hughes MJ (2016) Stochastic inversion by matching to large numbers of pseudo-wells. Geophysics 81(2):M7–M22

Corradin C (2025) Hydrogeological model of the Venetian-Friulian Plain and North Adriatic: assessing onshore dynamics and offshore availability. Doctoral Thesis, University of Trieste
Correggiari A, Field ME, Trincardi F (1996) Late quaternary transgressive large dunes on the sediment-starved Adriatic shelf. Geological Society, London, Special Publications 117(1):155–169
Covelli S, Piani R, Faganeli J, Brambati A (2004) Circulation and suspended matter distribution in a microtidal deltaic system: the Isonzo river mouth (northern Adriatic Sea). J Coastal Res 41:130–140
Cowan EJ, Beatson RK, Fright WR, McLennan TJ, Mitchell TJ (2002) Rapid geological modeling, Applied structural geology for mineral exploration and mining, international symposium (pp 23–25)
Cucchi F, Franceschini G, Zini L (2008) Hydrogeochemical investigations and groundwater provinces of the Friuli Venezia Giulia Plain aquifers, northeastern Italy. Environ Geol 55:985–999
Cuffaro M, Riguzzi F, Scrocca D, Antonioli F, Carminati E, Livani M, Doglioni C (2010) On the geodynamics of the northern Adriatic plate. RENDICONTI LINCEI 21:253–279
Da Lio C, Tosi L (2018) Land subsidence in the Friuli Venezia Giulia coastal plain, Italy: 1992–2010 results from SAR-based interferometry. Sci Total Environ 633:752–764
Da Lio C, Tosi L, Zambon G, Vianello A, Baldin G, Lorenzetti G, Manfè G, Teatini P (2013) Long-term groundwater dynamics in the coastal confined aquifers of Venice (Italy). Estuar Coast Shelf Sci 135:248–259
Dal Cin M, Böhm G, Busetti M, Picotti S, Zgur F, Camerlenghi A (2022) 3D velocity-depth model from multichannel seismic in the Dinaric foredeep of the Gulf of Trieste (Adriatic Sea), at the NE edge of Adria plate. Tectonophysics 838:229470. https://doi.org/10.1016/j.tecto.2022.229470
Deutsch CV, Journel AG (1992) Geostatistical software library and user's guide. N Y 119(147):578
Dercourt J, Zonenshain LP, Ricou L-E, Kazmin VG, Le Pichon X, Knipper AL, Grandjacquet C, Sbortshikov IM, Geyssant J, Lepvrier C, Pechersky DH, Boulin J, Sibuet J-C, Savostin LA, Sorokhtin O, Westphal M, Bazhenov ML, Lauer JP, Biju-Duval B (1986) Geological evolution of the tethys belt from the atlantic to the pamirs since the LIAS. Tectonophysics 123:241–315. https://doi.org/10.1016/0040-1951(86)90199-X
Donda F, Civile D, Forlin E, Volpi V, Zecchin M, Gordini E, Merson B, De Santis L (2013) The northernmost Adriatic Sea: a potential location for CO2 geological storage? Mar Pet Geol 42:148–159. https://doi.org/10.1016/j.marpetgeo.2012.10.006
Dunne T (1983) Relation of field studies and modeling in the prediction of storm runoff. J Hydrol 65(1–3):25–48
Durán O, Moore LJ (2013) Vegetation controls on the maximum size of coastal dunes. Proc Natl Acad Sci U S A 110(43):17217–17222
Fontana A, Mozzi P, Bondesan A (2008) Alluvial megafans in the Veneto-Friuli Plain: evidence of aggrading and erosive phases during late Pleistocene and Holocene. Quat Int 189:71–89
Fontana A, Mozzi P, Bondesan A (2010) Late pleistocene evolution of the Venetian-Friulian Plain. RENDICONTI LINCEI 21:181–196
Fontana A, Bondesan A, Meneghel M, Toffoletto F, Vitturi A, Bassan V (eds) (2012) Note illustrative della Carta Geologica d'Italia alla scala 1:50.000 Foglio 107 — Portogruaro. ISPRA-Regione del Veneto, Roma, p 168
Fontolan G, Pillon S, Bezzi A, Villalta R, Lipizer M, Triches A, D'Aietti A (2012) Human impact and the historical transformation of saltmarshes in the Marano and Grado Lagoon, northern Adriatic Sea. Estuar Coast Shelf Sci 113:41–56. https://doi.org/10.1016/j.ecss.2012.02.007
Giustiniani M, Busetti M, Dal Cin M, Barison E, Cimolino A, Brancatelli G, Baradello L (2022) Geophysical and geological views of potential water resources in the North-eastern Adriatic Sea. Geosciences 12:139. https://doi.org/10.3390/geosciences12030139
Goswami G, Basack S, Mastorakis N, Saikia A, Nilo B, Ahmed N (2020) Coastal ground water flow and management: a state-of-the-art review. Int J Mech 14:37–48
Horton RE (1940) An approach toward a physical interpretation of infiltration capacity. In: Soil science society of America proceedings, vol 5, no. 399–417. p 24
Liu H, Wu Y, Cao Y, Lv W, Han H, Li Z, Chang J (2020) Well logging based lithology identification model establishment under data drift: a transfer learning method. Sensors 20(13):3643
Livani M, Petracchini L, Benetatos C, Marzano F, Billi A, Carminati E, Doglioni C, Petricca P, Maffucci R, Codegone G, Rocca V, Verga F, Antoncecchi I (2023) 2023), subsurface geological and geophysical data from the Po Plain and the northern Adriatic Sea (north Italy. Earth Syst Sci Data 15:4261–4293. https://doi.org/10.5194/essd-15-4261-2023
Lobo FJ, Ridente D (2014) Stratigraphic architecture and spatio-temporal variability of high-frequency (Milankovitch) depositional cycles on modern continental margins: an overview. Mar Geol 352:215–247. https://doi.org/10.1016/j.margeo.2013.10.009
Lorenzo-Trueba J, Ashton AD (2014) Rollover, drowning, and discontinuous retreat: distinct modes of barrier response to sea-level rise arising from a simple morphodynamic model. J Geophys Res Earth Surf 119:779–801. https://doi.org/10.1002/2013JF002941
Malanotte-Rizzoli PM, Robinson AR (eds) (2012) Ocean processes in climate dynamics: global and Mediterranean examples, vol 419. Springer, Berlin
Maliva RG (2016) Geostatistical methods and applications. In: Aquifer characterization techniques: Schlumberger methods in water resources evaluation series no. 4. Springer International Publishing, Cham, pp 595–617
Mancin N, Cobianchi M, Di Giulio A, Catellani D (2007) Stratigraphy of the Cenozoic subsurface succession of the Venetian-Friulian Basin (NE Italy): a review. Riv Ital Paleontol Stratigr 113(3):401
Marchesini A, Poli ME, Bonini L, Busetti M, Piano C, Dal Cin M, Paiero G, Areggi G, Civile D, Ponton M, Patricelli G, Tamaro A and the working group 'Faglie Attive FVG, 2023' (2023) Linee guida per l'utilizzo della banca georiferita delle faglie attive della Regione Friuli Venezia Giulia. Gelogical Survery - Autonomous region Friuli Venezia Giulia, 64 pp
Marcolla A, Miola A, Mozzi P, Monegato G, Asioli A, Pini R, Stefani C (2021) Middle Pleistocene to Holocene palaeoenvironmental evolution of the south-eastern Alpine foreland basin from multiproxy analysis. Quat Sci Rev 259:106908. https://doi.org/10.1016/j.quascirev.2021.106908
Martelli G, Granati C (2006) The confined aquifer system of Friuli Plain (North Eastern Italy): analysis of sustainable groundwater use. G Geol Appl 3:59–67
Martinson DG, Pisias NG, Hays JD, Imbrie J, Moore TC Jr, Shackleton NJ (1987) Age dating and the orbital theory of the ice ages: development of a high-resolution 0 to 300,000-year chronostratigraphy1. Quat Res 27(1):1–29
Massari F, Rio D, Serandrei Barbero R, Asioli A, Capraro L, Fornaciari E, Vergerio PP (2004) The environment of Venice area in the past two million years. Palaeogeogr Palaeoclimatol Palaeoecol 202:273–308. https://doi.org/10.1016/S0031-0182(03)00640-0
Lipparini L, Chiacchieri D, Bencini R, Micallef A (2023) Extensive freshened groundwater resources emplaced during the Messinian sea-level drawdown in southern Sicily Italy. Commun Earth Environ 4(1):430
Micallef A, Person M, Haroon A, Weymer BA, Jegen M, Schwalenberg K, Faghih Z, Duan S, Cohen D, Mountjoy JJ, Woelz S, Gable CW, Averes T, Kumar Tiwari A (2020) 3D characterisation and quantification of an offshore freshened groundwater system in the Canterbury Bight. Nat Commun 11(1):1372

Micallef A, Person M, Berndt C, Bertoni C, Cohen D, Dugan B, Evans R, Haroon A, Hensen C, Jegen M, Key K, Kooi H, Liebetrau V, Lofi J, Mailloux BJ, Martin-Nagle R, Michael HA, Müller T, Schmidt M, Schwalenberg K, Trembath-Reichert E, Weymer B, Zhang Y, Thomas AT (2021) Offshore freshened groundwater in continental margins. Rev Geophys 59:e2020RG000706. https://doi.org/10.1029/2020RG000706

Morgan LK, Mountjoy JJ (2022) Likelihood of offshore freshened groundwater in New Zealand. Hydrogeol J 30(7):2013–2026. https://doi.org/10.1007/s10040-022-02525-1

Palano M (2015) On the present-day crustal stress, strain-rate fields and mantle anisotropy pattern of Italy. Geophys J Int 200:969–985. https://doi.org/10.1093/gji/ggu451

Pezzetta E, Lutman A, Martinuzzi I, Viola C, Bernardis G, Fuccaro V (2011) Iron concentrations in selected groundwater samples from the lower Friulian plain, Northeast Italy: importance of salinity. Environ Earth Sci 62(2):377–391

Piva A, Asioli A, Schneider RR, Trincardi F, Andersen N, Colmenero-Hidalgo E, Dennielou B, Flores J-A, Vigliotti L (2008) Climatic cycles as expressed in sediments of the PROMESS1 borehole PRAD1-2, central Adriatic, for the last 370 ka: 1. Integrated stratigraphy. Geochem Geophys Geosyst. https://doi.org/10.1029/2007GC001713

Post VEA, Groen J, Kooi H, Person M, Ge S, Edmunds WM (2013) Offshore fresh groundwater reserves as a global phenomenon. Nature 504:71–78. https://doi.org/10.1038/nature12858

Pyrcz MJ, Deutsch CV (2014) Geostatistical reservoir modelling. Oxford University Press

Rabineau M, Berné S, Olivet J-L, Aslanian D, Guillocheau F, Joseph P (2006) Paleo sea levels reconsidered from direct observation of paleoshoreline position during glacial maxima (for the last 500,000 yr). Earth Planet Sci Lett 252:119–137. https://doi.org/10.1016/j.epsl.2006.09.033

Ridente D, Trincardi F (2002) Eustatic and tectonic control on deposition and lateral variability of Quaternary regressive sequences in the Adriatic basin (Italy). Mar Geol 184(2002):273–293

Robertson AHF, Grasso M (1995) Overview of the late tertiary-recent tectonic and palaeo-environmental development of the Mediterranean region. Terra Nova 7:114–127. https://doi.org/10.1111/j.1365-3121.1995.tb00680.x

Ronchi L, Fontana A, Correggiari A, trans (2018) Characteristics and potential application of Holocene tidal inlets in the northern Adriatic shelf (Italy), Alpine and Mediterranean Quaternary, pp 31–34. https://amq.aiqua.it/index.php/amq/article/view/182

Russo A, Artegiani A (1996) Adriatic Sea hydrography. Sci Mar 60:33–43

Shackleton NJ (1997) The deep-sea sediment record and the Pliocene-Pleistocene boundary. Quat Int 40:33–35

Sheng C, Jiao JJ, Luo X, Zuo J, Jia L, Cao J (2023) Offshore freshened groundwater in the Pearl River estuary and shelf as a significant water resource. Nat Commun 14(1):3781

Storms JE, Weltje GJ, Terra GJ, Cattaneo A, Trincardi F (2008) Coastal dynamics under conditions of rapid sea-level rise: late Pleistocene to early Holocene evolution of barrier–lagoon systems on the northern Adriatic shelf (Italy). Quat Sci Rev 27(11–12):1107–1123

Thomas AT, Reiche S, Riedel M, Clauser C (2019) The fate of submarine fresh groundwater reservoirs at the New Jersey shelf, USA. Hydrogeol J 27:2673–2694. https://doi.org/10.1007/s10040-019-01997-y

Trincardi F, Correggiari A (2000) Quaternary forced regression deposits in the Adriatic basin and the record of composite sea-level cycles. SP 172:245–269. https://doi.org/10.1144/GSL.SP.2000.172.01.12

UN Water (Ed.) (2022) Groundwater making the invisible visible. The United Nations world water development report. UNESCO, Paris

Vai GB, Cantelli L, Antonioli F (2004) Litho-palaeoenvironmental maps of Italy during the last two climatic extremes. Museo archeologico Giovanni Capellini

Vdovic N, Juracic M (1993) Sedimentological and surface characteristics of the Northern and Central Adriatic sediments. Geol Croat 46(1):157–163

Webster R, Oliver MA (2007) Geostatistics for environmental scientists. Wiley, Chichester. https://doi.org/10.1002/9780470517277

Wolff RG (1982) Physical properties of rocks; porosity, permeability, distribution coefficients, and dispersivity (No. 82–166). US Geological Survey

Zanferrari A, Avigliano R, Fontana A, Paiero G, (Eds.) (2008) Note Illustrative della Carta Geologica d'Italia alla scala 1:50.000 Foglio 087 San Vito al Tagliamento. Graphic Linea, Tavagnacco, Udine, p 178

Zavagno E, Zini L, Cucchi F (2015) Saltwater intrusion in Friuli Low Plain. Georisks in the Mediterranean and their Mitigation, p 205. International Conference University of Malta - Valletta Campus 20-21 July 2015

Zecchin M, Busetti M, Donda F, Dal Cin M, Zgur F, Brancatelli G (2022) Plio-Quaternary sequences and tectonic events in the northern Adriatic Sea (northern Italy). Mar Pet Geol 142:105745. https://doi.org/10.1016/j.marpetgeo.2022.105745

Zecchin M, Donda F, Forlin E (2017) Genesis of the Northern Adriatic Sea (Northern Italy) since early Pliocene. Mar Pet Geol 79:108–130. https://doi.org/10.1016/j.marpetgeo.2016.11.009

Zecchin M, Gordini E, Ramella R (2015) Recognition of a drowned delta in the northern Adriatic Sea, Italy: stratigraphic characteristics and its significance in the frame of the early Holocene sea-level rise. Holocene 25:1027–1038. https://doi.org/10.1177/0959683615575358

Zini L, Calligaris C, Treu F, Iervolino D, Lippi F (2011) Risorse idriche sotterranee del Friuli Venezia Giulia: sostenibilità e utilizzo

Zini L, Calligaris C, Treu F, Zavagno E, Iervolino D, Lippi F (2023) Groundwater sustainability in the Friuli Plain. As-ITJGW 12:77–92. https://doi.org/10.7343/as-2023-713